RF sputtered NiO_x as hole transport layer of $CH_3NH_3PbI_3$ perovskite solar cells

Key Words: Solar cells, Photovoltaics, Perovskite, NiO

Introduction

NiO has been used as hole transport layers of $CH_3NH_3PbI_3$ perovskite (PVK) solar because of its large bandgap (E_g), deep valence band maximum (VBM=5.4 eV), favorable energy level alignment with a deep-lying VBM of PVK. We have demonstrate high stability of inverted planar PVK solar cells on the basis of the sputter-deposited NiO_X. We characterize and discuss the surface properties of NiO_X prepared at various powers of the RF sputtering machine.

Theme under Discussion

RF sputtering methods have been used as powerful tools for making thin layer photovoltaics such as CIGS and thin films Si solar cells because the methods are quick to prepare the thin layered insulator or semiconductor materials. However, the long sputtering time (over 2h) is needed to prepare NiO_X films (over 30 nm) now. We need to characterize the properties of NiO_X prepared at various powers of the RF machine to enhance the speed of the preparation.

Perovskite(PVK) solar cells

Device structure of inverted $CH_3NH_3PbI_3$ perovskite (PVK) solar cells NiOx layer is prepared by sputtering method.

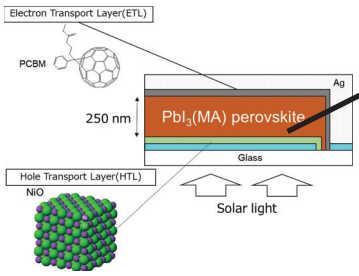

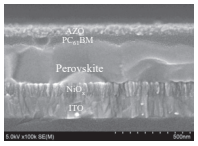

Cross section SEM image of PVK solar cells

NiOx sputtered layer

RF sputtering of NiOx

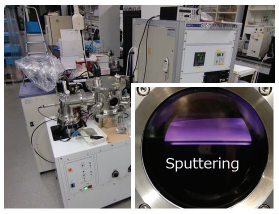

Condition
Target material : NiO
Pressure : 3.5 Pa
Temperature : Room
Power : 50W, 100W, 200W
Time : 15min-3 hours

SEM images of the surface of NiO_x prepared at various RF power.

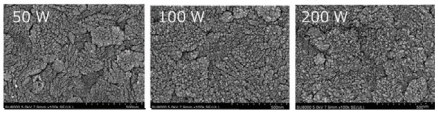

XRD pattern of NiO_x layer on ITO prepared at various RF power.

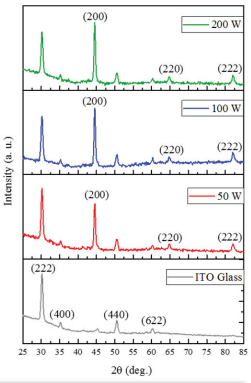

Conclusion

1, The lower V_{OC} with increase of the power is due to the higher shifted *WF*.
2,The XP peaks of O1s at 531.3 eV, assigned to $Ni(OH)_2$ decreases with increase of the power.
3, The decrease of OH groups in NiO_X shifts the *WF* to higher energy.

Photovltaic properties

***J-V* curve of PVK solar cells**

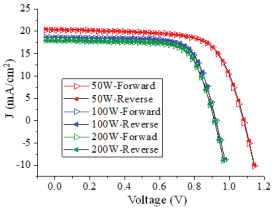

Work function(WF) of NiOx vs. sputtering power

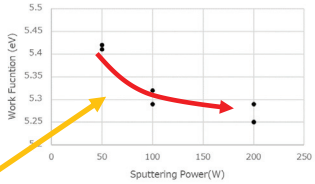

***J-V* properties of PVK's**

Power (W)	η (%)	J_{sc} (mA/cm²)	V_{oc} (V)	FF	Rs (Ω·cm²)	R_{sh}x10³ (Ω·cm²)
50	15.0	19.97	1.09	0.69	6.0	3.25
100	12.2	18.20	0.93	0.72	5.7	2.36
200	11.0	17.29	0.91	0.70	6.0	1.85

Shunt resistances (R_{sh}) of PVK solar cells based are almost same at various sputtering powers .

Surface properties of NiOx

Power depedent XP spectra of O_{1s} normalized at 529.4 eV(NiO)

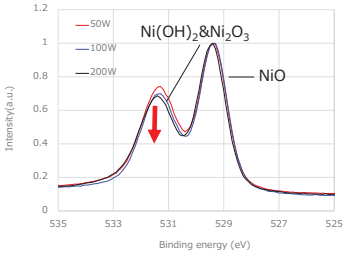

Scheme of the relationship between Voc and shift of WF

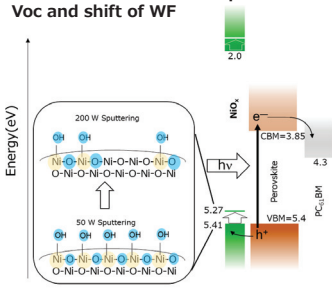

Reference: (1) Yanagida et. al, Electrochemistry **85**, 231 (2017).
(2) Islam et. al, ACS Omega **2**, 2291(2017).(3) Jpn. J. Appl. Phys. **57**, 08RE06(2018).

Future Plan

Detail characterization of NiOx layer after RF supttering

- Understanding in higher power sputtering of NiO_x
- Checking other factors such as defect sites, mobility and so on.
- Surface treatment or modification of the NiO_X

ad hoc team on Perovskite PV Cells, GREEN Masatoshi Yanagida

E-mail: YANAGIDA.Masatoshi@nims.go.jp

Li concentration change around the electrode/glass electrolyte interface

Key Words: All-Solid-State Battery, Interface

Introduction

Details on electrode-solid electrolyte interface must be clarified well to improve the rate capability of all-solid-state rechargeable lithium batteries. We have investigated voltage dependencies of Li^+ concentration around the electrode/Li^+ conductive glass electrolytes interface using elastic recoil detection (ERD).

Theme under Discussion

Cyclic voltammetry (CV) and AC impedance spectroscopy (EIS) were carried out to investigate the interfacial resistances between electrodes and solid electrolytes. Also, ERD was carried out to evaluate the lithium concentration change around the interface against the base voltage (0 V).

Charge transfer resistance (R_{ct})

Samples

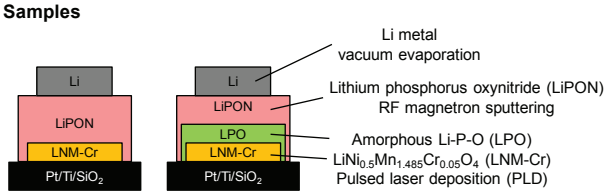

Cyclic voltammetry (CV)

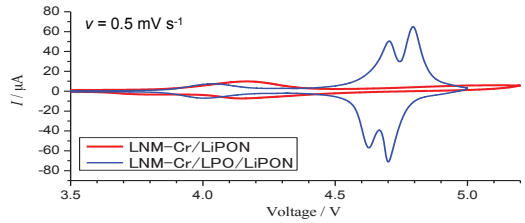

AC impedance epectroscopy (EIS)

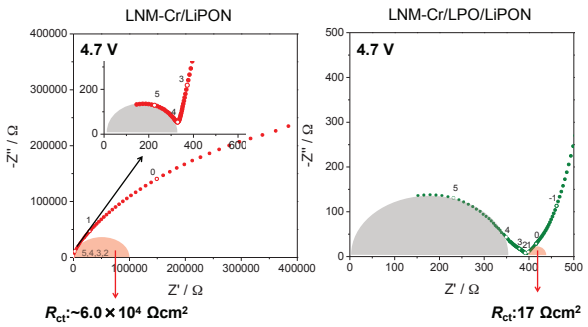

Both the CV and EIS results of thin film batteries show that interfacial resistance between LNM-Cr and LPO is much smaller than that between LNM-Cr and LiPON.

Li concentration change

Elastic Recoil Detection (ERD)

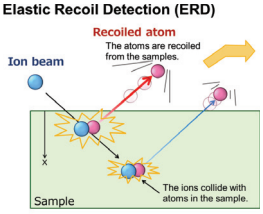

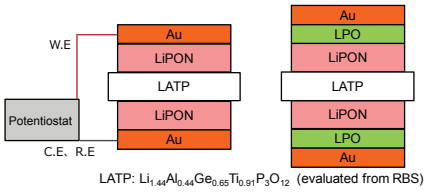

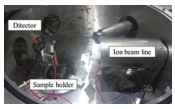

ERD analysis chamber
(Kyoto University)

ERD (Shielding non-target atoms)

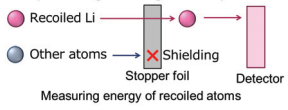

Au/LiPON/LATP/LiPON/Au

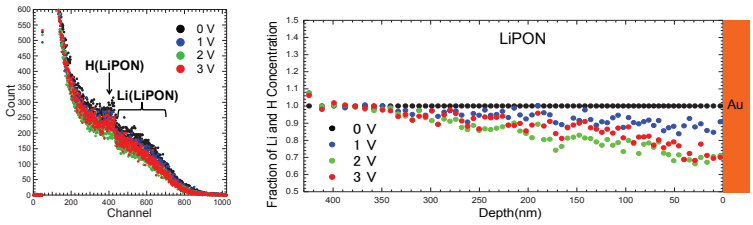

Au/LPO/LiPON/LATP/LiPON/LPO/Au

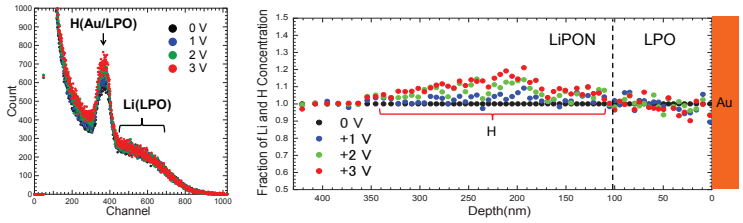

The Li^+ concentration of LPO is not observed in the ERD measurements while clear Li^+ concentration change of LiPON is detected with increasing the applied voltage.

Conclusion

The CV curves of the Li/LPO/LNM-Cr thin film battery showed sharp peaks although that of the Li/LiPON/LNM-Cr thin film battery provided broad ones. EIS data indicates that interfacial resistance between LNM-Cr and LPO is much smaller than that between LNM-Cr and LiPON. Such small interfacial resistance may be explained by the difference of Li^+ concentration at the interface between electrode and electrolyte. The ERD analysis indicates that the Li^+ concentration of LPO does not change deeply inside the solid electrolyte while that of LiPON changes with increasing the applied voltage.

Future Plan

The accurate Li^+ concentration change is still unclear due to the presence of hydrogen. Then we are planning to remove hydrogen from the samples to understand the relationship between the interfacial resistance and the Li^+ concentration more deeply.

Department of Materials Design Innovation Engineering, Nagoya University

Yasutoshi Iriyama, E-mail: iriyama.yasutoshi@material.nagoya-u.ac.jp

Study on carrier separation in perovskite solar cells by operando profiling of electrical potential distribution

Key Words: Kelvin probe force microscopy, Perovskite solar cell

Introduction

Perovskite solar cells (PSCs) are the most promising next generation photovoltaic technology, whose energy conversion efficiency has increased rapidly in a few years. However, in contrast to the rapid increase in efficiency, the fundamental understanding of the device working principles has hardly progressed. It is therefore important to clarify the details of photovoltaic conversion processes for a deeper understanding of the energy loss mechanism.

This work

Here we present a study of carrier separation processes in the PSCs by operando profiling of electrical potential distribution using Kelvin probe force microscopy (KPFM). We found that the position of the carrier separation in the PSCs depended on the device structures and the composition of the perovskite films. Our experimental findings suggested that controlling electrical potential distribution in PSCs was important in achieving high efficiency cells.

Results & Discussion

KPFM measurements on cross-sectional surface

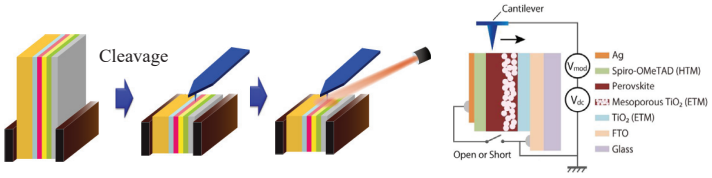

Identifying the position of p-n junction

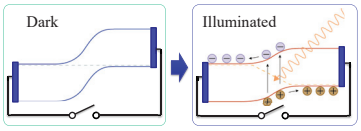

Device structure

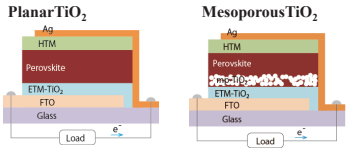

KPFM measurement under light irradiation conditions

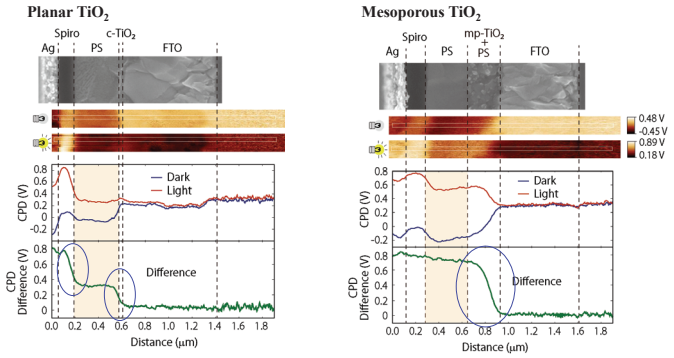

Dependence of potential distribution on the composition of perovskite film

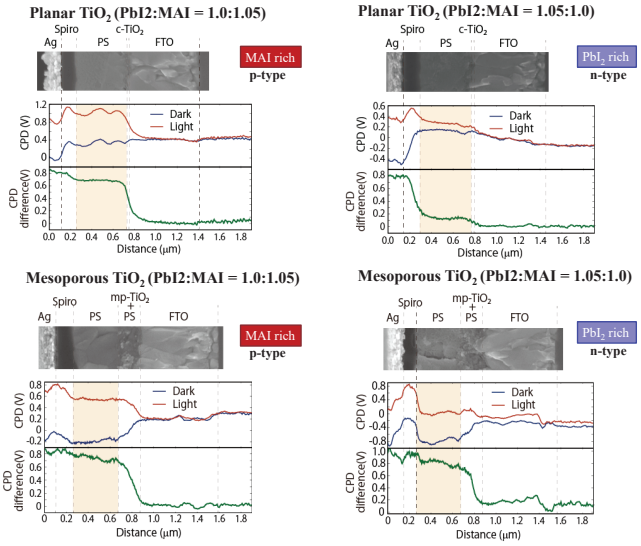

Comparison with macroscopic device performance

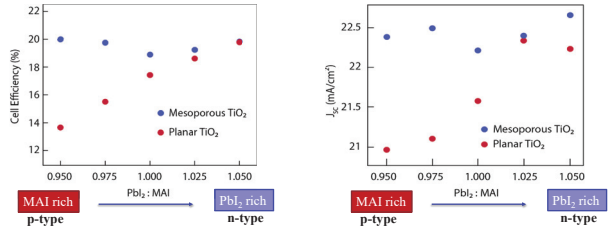

Conclusion

- We succeeded in visualizing the change of potential distribution in the PSCs induced by light irradiation using operando KPFM measurements.
- From the information of the potential distribution obtained, we considered the carrier separation process and the position of p-n junction in the PSCs.
- We found that the position of p-n junction (the position where carrier separation occurs) strongly depended on the device structure and the composition of perovskite films.
- Our results suggested that controlling the position of p-n junction through the device structure and/or composition of perovskite film is the key to improving device performance.

*1 NIMS-GREEN, *2 NIMS
Nobuyuki Ishida*1,2, Molang Cai*2, Takeshi Noda*2, Daisuke Fujita*1,2, and Liyuan Han*2
E-mail: ISHIDA.Nobuyuki@nims.go.jp

Incorporation of Multinuclear Metal Active Sites into Nitrogen-doped Graphene for Electrochemical Reactions

Key Words: Oxygen reduction reaction; Electrocatalyst; Polymer electrolyte fuel cells

Introduction

Metalloenzymes show high catalytic activity and utilize multinuclear metal active sites as catalytic reaction centers. The incorporation of multinuclear metal centers in conductive materials such as carbon would produce highly active non-platinum-group-metal electrocatalysts. However, there is a lack of synthetic strategies on such electrocatalysts.

Theme under Discussion

Multinuclear metal active sites, inspired by active sites of metalloenzymes, were incorporated into nitrogen-doped graphene for the electrochemical oxygen reduction reaction (ORR) in pyrolysis. The pyrolytic synthesis also provided Co/N/C electrocatalysts, which shows catalytic activity for the ORR and the electrochemical oxidation of lignin model compounds.

Cu/N/C electrocatalysts

Laccase

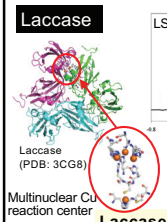

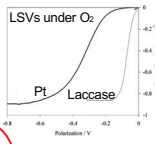

Mano, *et al.*, *J. Phys. Chem. B*, **110**, 11180-11187 (2006).

Laccases are more active than Pt for the ORR.

Synthesis: laccase-inspired catalysts

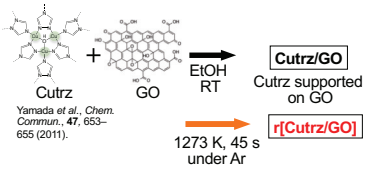

Yamada *et al.*, *Chem. Commun.*, **47**, 653–655 (2011).

Linear sweep voltammetry under oxygen

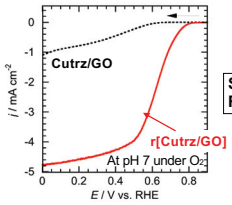

Sweep rate: 0.02 V s^{-1};
Revolution rate: 1600 rpm

Cu,N-codoping into carbon is the key to prepare the highly active ORR catalyst.

Cu L_3-edge X-ray Absorption Spectroscopy

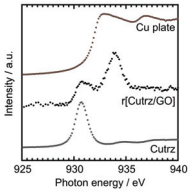

Recorded under vacuum in a total fluorescent yield method.

r[Cutrz/GO] contains Cu^{II} and Cu^{I}.

HAADF-STEM image

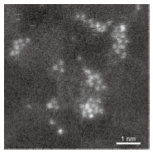

Taken by using JEOL JEM-ARM200F at 80 kV

r[Cutrz/GO] contains multinuclear copper active sites.

In situ Cu *K*-edge XAFS

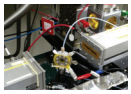

In situ XAFS flow cell
M. Kato *et al.*, *PCCP*, **17**, 8638-8641 (2015).

FT-EXAFS under O2

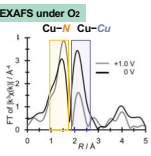

Atom	C.N.	Distance / Å
+1.0 V under oxygen		
N	2.6±0.4	1.93±0.01
Cu	0.4±0.1	2.61±0.02
0 V under oxygen		
N	2.3±0.5	1.87±0.02
Cu	1.4±0.5	2.55±0.02

C.N. = coordination number

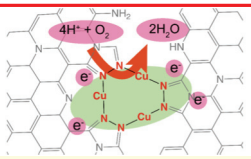

Multinuclear Cu^{I} cores work as active sites for the ORR.

Kato *et al.*, *ACS Appl. Energy Mater.*, **1**, 2358-2364 (2018).

Fe/Cu/N/C electrocatalysts

Cytochrome *c* oxidase

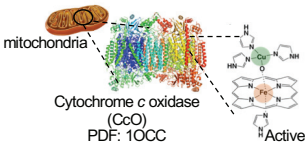

Synthesis: CcO-inspired catalysts

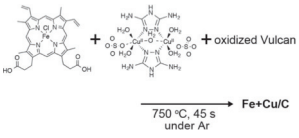

Linear sweep voltammetry under oxygen

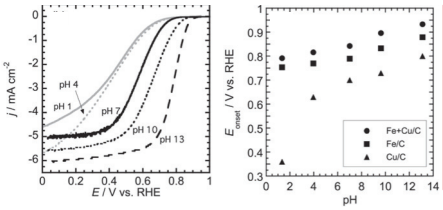

The co-presence of Cu and Fe active sites shows higher electrocatalytic activity for the ORR.

Kato, Murotani, Yagi, *Chem. Lett.*, **45**, 1213–1215 (2016).

Co/N/C electrocatalysts

Synthesis: Co/N/C electrocatalysts

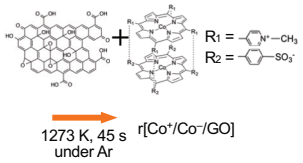

TEM & XAFS

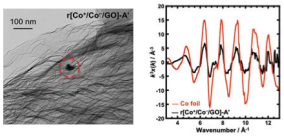

Linear sweep voltammetry for the ORR

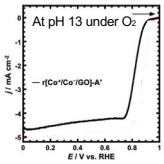

Sweep rate: 0.01 V s^{-1};
Revolution rate: 1600 rpm
Electrolyte solution: 0.1 M KOH

Electrochemical oxidation of lignin and its model compounds

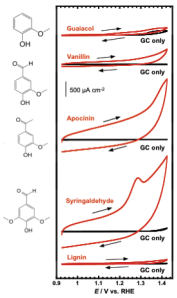

Co/N/C shows electrocatalytic activity not only for the ORR but also electrochemical oxidation of lignin model compounds.

Faculty of Environmental Earth Science, Hokkaido University Masaru Kato and Ichizo Yagi

E-mail: masaru.kato@ees.hokudai.ac.jp

Discharge/charge cycling of Lithium-Air Battery cells with ultra-high capacity CNT cathode

Key Words: Lithium-Air Battery, air electrode, carbon nanotube

Introduction

Rechargeable battery plays a crucial roles in the popularization of electric vehicles and renewable energy. Current lithium-ion battery (LiB) technologies are getting their theoretical limits, thus alternative technologies need to be developed. Lithium-air battery (LAB) is one of the promising candidates of the post lithium-ion in terms of much higher energy density (10 times or more than LiB) that could be produced with competitive cost.

Theme under Discussion

LAB is expected to develop a cell with huge capacity, but the present LAB cells exhibit less cell capacity than theoretically expected (typically <10 mAh/cm^2). Thanks to the flexible but tough bundle structure of carbon nanotube (CNT), the sheet as air electrode develops ultra-high cell capacity of 30 mAh/cm^2 or more. LAB secondary battery with high energy density (>500 Wh/kg target) is under development using the CNT sheet cathode.

CNT sheet air electrode in LAB cell

LAB coin-cell using CNT sheet as air electrode.

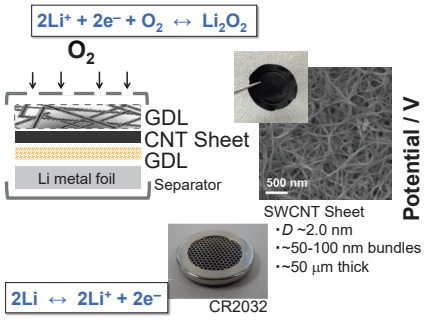

The cells discharge **up to 86 mAh/cm^2**
(while present LiB cells have ~2 mAh/cm^2 areal capacity).

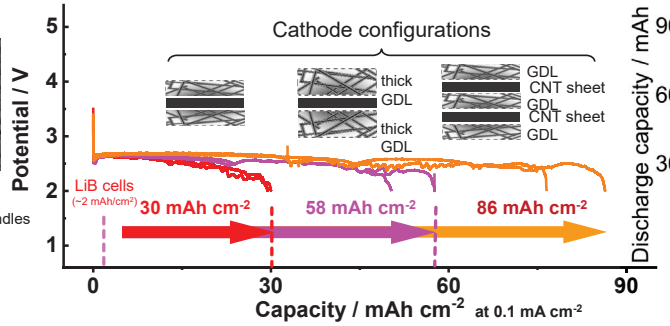

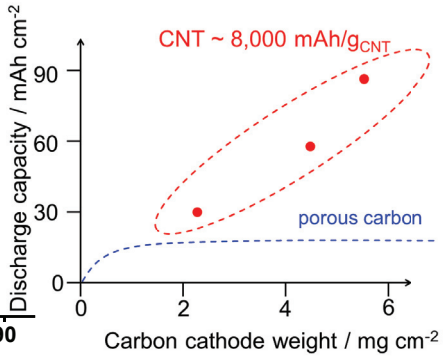

Discharge/charge cycle property of LAB cell with CNT sheet cathode

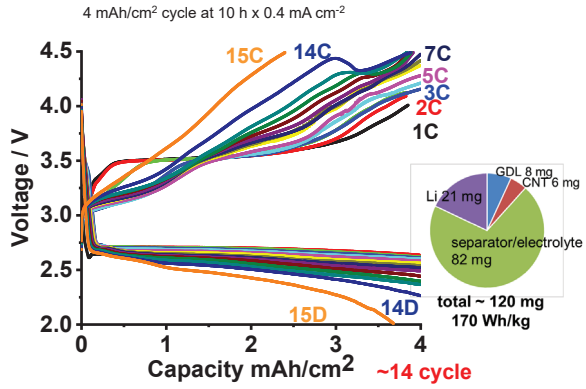

Electrodes after discharge/charge cycling

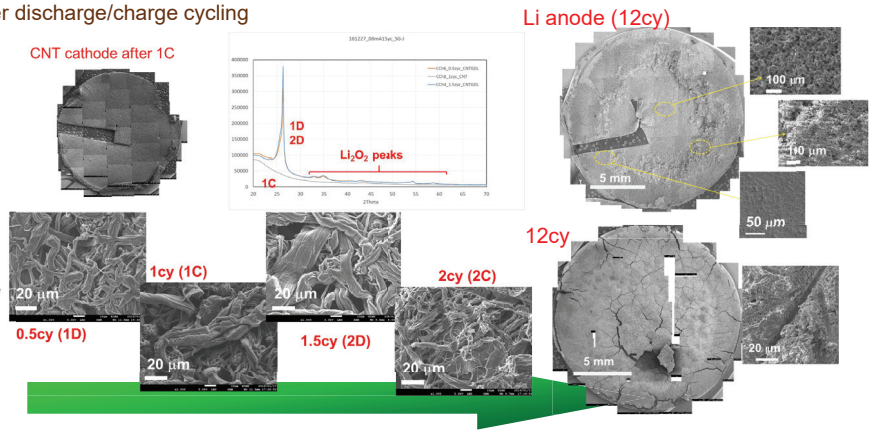

Conclusion

- CNT sheet air electrode develops LAB cells with ultra-high cell capacity of 30 mAh/cm^2 or more, which is 15 times higher than current lithium-ion technologies.
- LAB cell with the CNT sheet cathode at present develops 170Wh/kg battery that can discharge/charge about 10.

Future Plan

- Understanding the degradation process of CNT cathode and Li anode during discharge/charge cycling.
- Fabrication of highly porous, lightweight, thin bundle CNT sheet for the development of huge energy density battery.
- Establishing air purification system to allow atmospheric battery operation of the LAB cells.

Lithium-Air Battery Specially Promoted Research Group, GREEN Akihiro Nomura

E-mail: NOMURA.Akihiro@nims.go.jp

Electrode potential and charge transfer reaction using ESM-RISM calculations

Jun Haruyama Institute for Solid State Physics (ISSP), The University of Tokyo haruyama@issp.u-tokyo.ac.jp

Introduction

½ H_2(gas) + H_2O(S) ↔ H_3O^+(S) + e^-(M) : Standard Hydrogen Electrode (SHE)

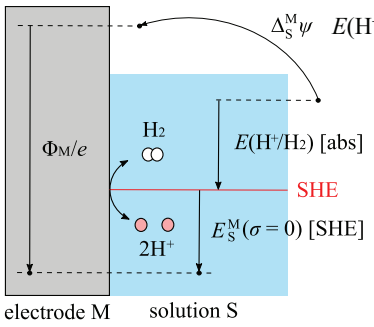

(1) S. Trasatti, *Pure Appl. Chem.* **58**, 955 (1986).

Φ_M : work function

$\Delta_S^M\psi$: contact potential difference

$E_S^M(\sigma=0)$[SHE]
: potential of zero charge (PZC)

Li_nC_{6m} (electrode) ⇔ $Li_{n-1}C_{6m}$ (electrode) + Li^+ (solvated)

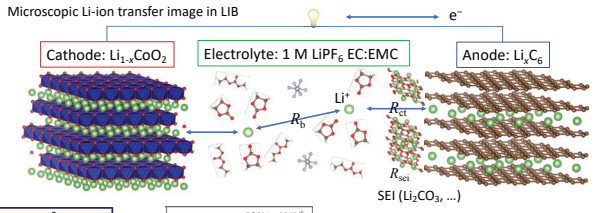

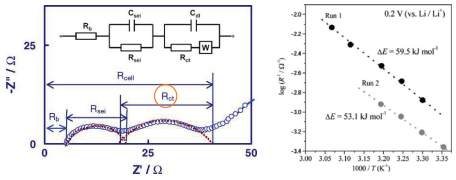

(2) S. S. Zhang, K. Xu, and T. R. Jow, *Electrochem. Acta* **49**, 1057 (2004).
(3) T. Abe, H. Fukuda, Y. Iriyama, and Z. Ogumi, *J. Electrochem. Soc.* **151**, A1120 (2004).

Methods – ESM-RISM calculation

- DFT calculations combined with the effective screening medium (ESM)[4] technique + the reference interaction site model[5] (RISM) -> **ESM-RISM calculation**[6]
- **QM/MM** like approach { Electrode (+reacted ion) -> Quantum mechanics (QM); Electrolyte solution -> Implicit solvation (RISM) }

Grand canonical system μ_e, N_e : Chemical potential, number of electron
$\Omega \equiv A - \mu_e N_e$: Grand potential $A = E_{DFT} + \Delta A_{RISM}$: (Helmholtz) free energy

- The interaction between DFT and RISM is represented as electrostatic potential (v_{es}) and RISM classical force field (FF) potential (v_{solv}). $v_{tot}(\mathbf{r}) = v_{es}(\mathbf{r}) + v_{solv}(\mathbf{r})$

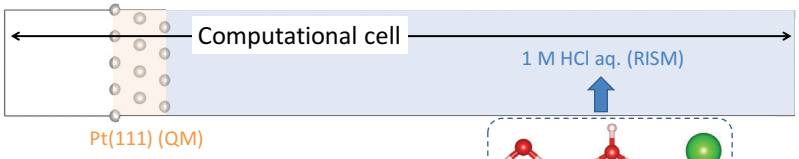

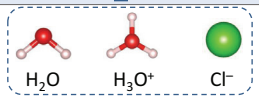

- ESM-RISM is Implemented in Quantum-Espresso package.[7]
- Electrons are added/excluded to reach the target μ_e, and the extra charge is compensated by ions in the solution.
➡The total charge is neutral; inner potential Φ_S can be defined.

Water distribution at Pt(111) surface

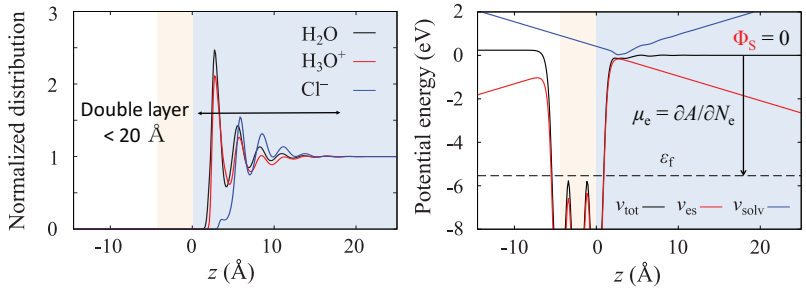

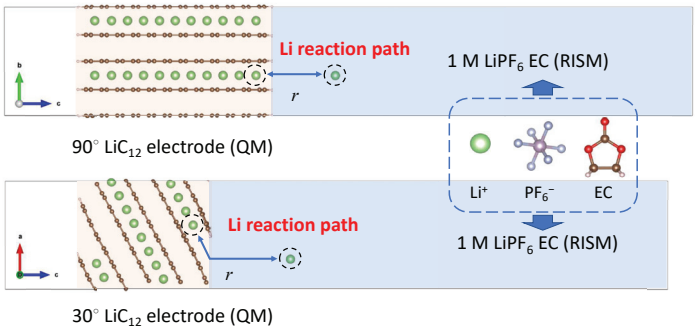

J. Haruyama, T. Ikeshoji, and M. Otani, *J. Phys. Chem. C* **122**, 9804 (2018).

(4) M. Otani and O. Sugino, *Phys. Rev. B* **73**, 115407 (2006). (5) A. Kovalenko and F. Hirata, *Chem. Phys. Lett.* **290**, 237 (1998). (6) S. Nishihara and M. Otani, *Phys. Rev. B* **96**, 115429 (2017). (7) P. Giannozzi et al., *J. Phys.: Condens. Matter.* **21**, 395502 (2009).

Results

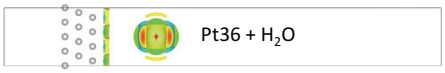

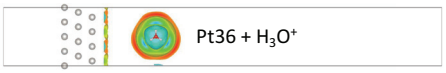

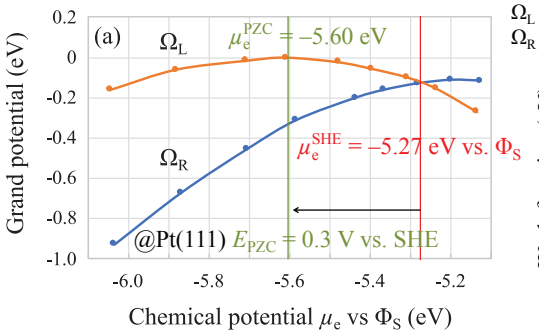

Ω_L = ½ A (H_2, gas) + Ω(Pt111 + H_2O/1 M HCl aq.)
Ω_R = Ω(Pt111 + H_3O^+/1 M HCl aq.)

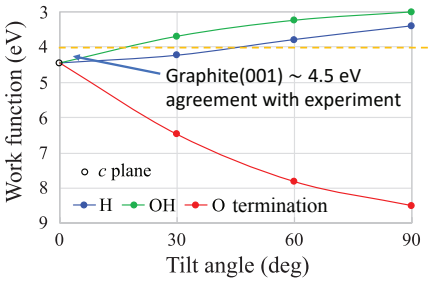

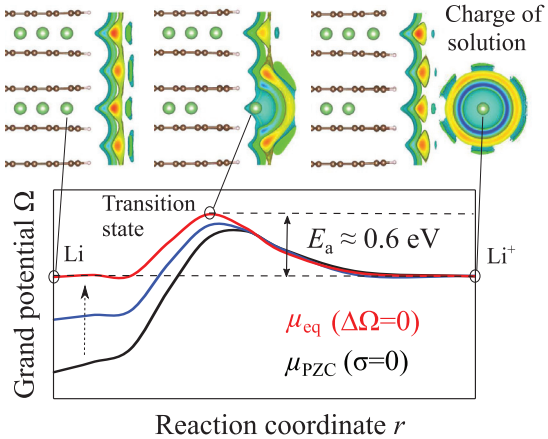

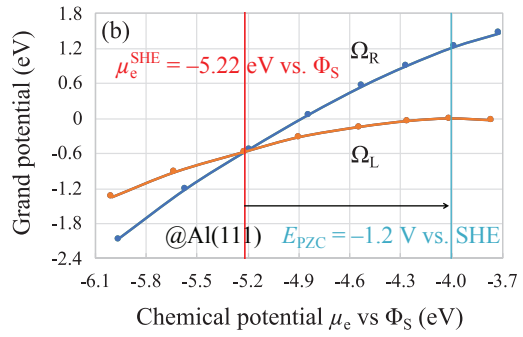

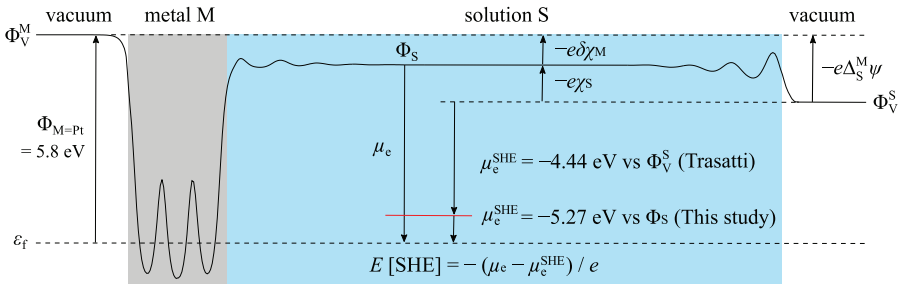

J. Haruyama, T. Ikeshoji, and M. Otani, *Phys. Rev. Mater.* **2**, 095801 (2018).

P-7

Highly Sulfonated Polyphenylsulfone Polymer for PEMFCs

Je-Deok Kim[1,2*]

[1]Hydrogen production materials group, [2]Polymer electrolyte fuel cell group, GREEN, NIMS, 1-1 Namiki, Tsukuba, Ibaraki 305-0044, Japan

*E-mail: Kim.jedeok@nims.go.jp

Introduction

Current situation of PEM fuel cells and hydrogen infra-market

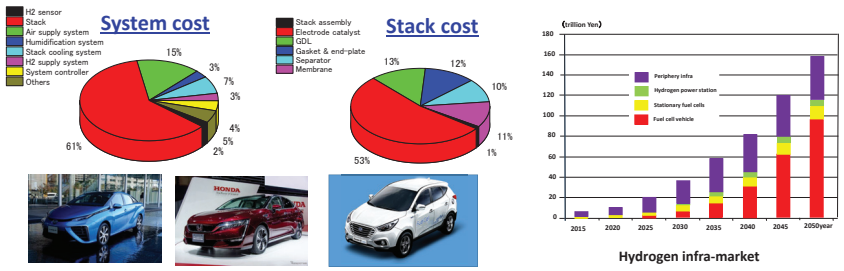

Research Topic: Super polymer development

Crosslinked SPPSU

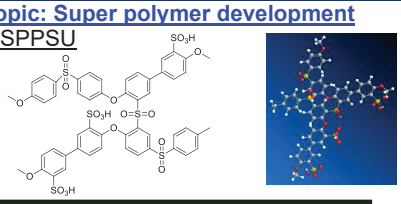

- @ Water soluble → diversity (water, alcohol, etc.)
- @ Crosslinking (annealing) → water insoluble
- @ High mechanical & chemical stability
- @ High conductivity

Experimental

Sulfonation of PPSU

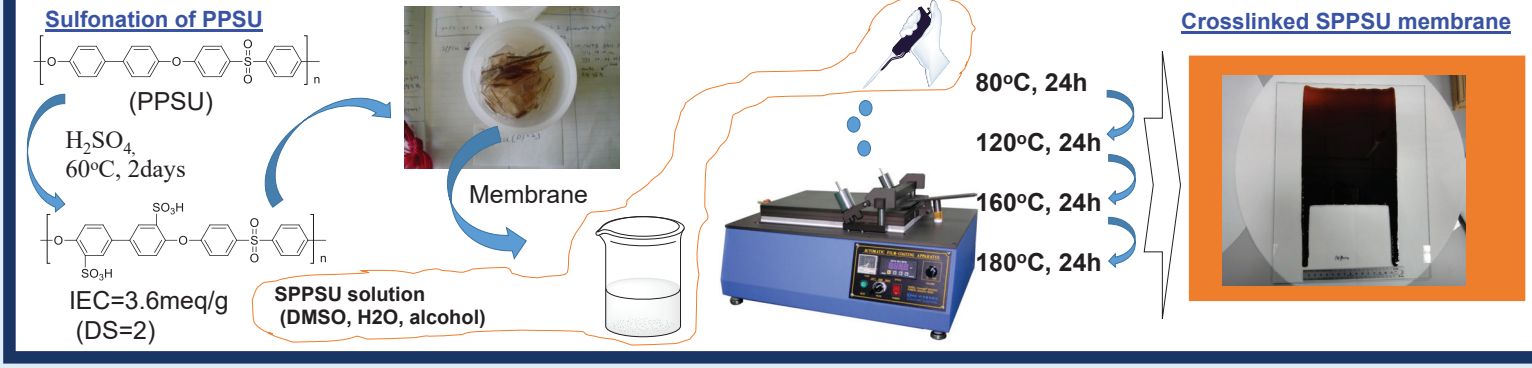

Results & Discussion

TGA, dynamic elastic modulus, tan δ, stress-strain, conductivity, I-V, and durability properties of crosslinked SPPSU membranes

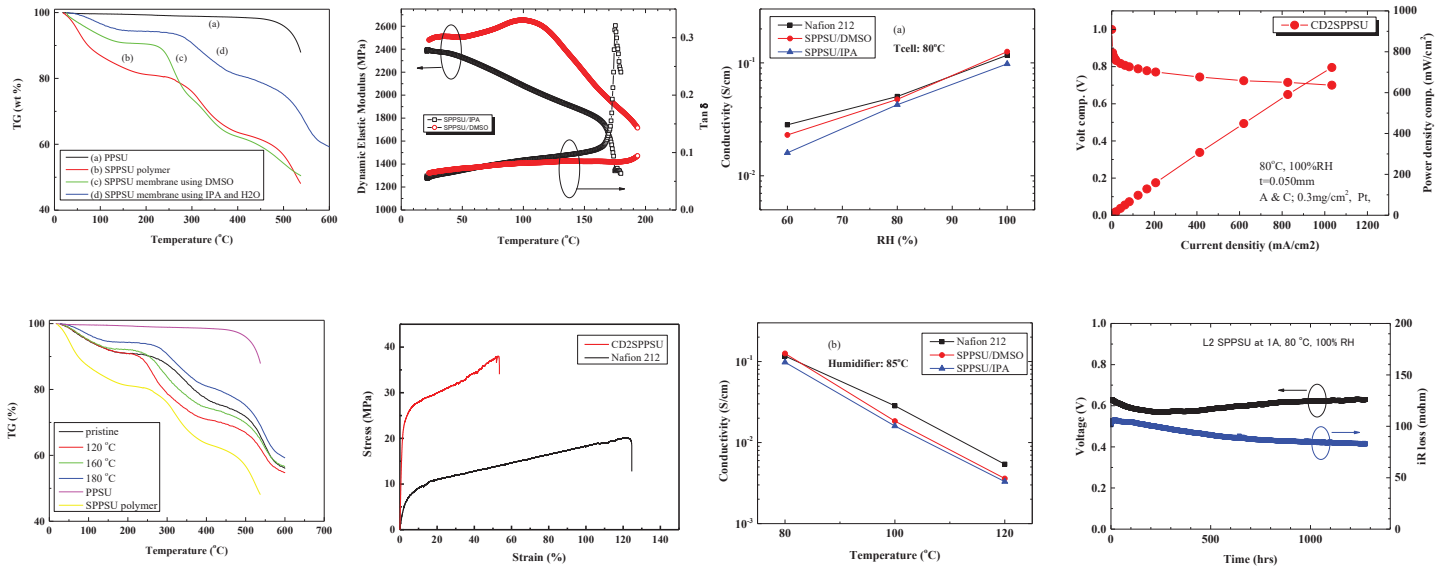

[1] **J.D. Kim**, L.-J. Ghil, "Annealing effect of highly sulfonated polyphenylsulfone polymer Int. J. Hydrogen Energy, **41**, 11794-11800 (2016) .

Conclusion

Objective:

- Development of hydrocarbon polymer electrolyte membrane

Methodology:

- High sulfonation using PPSU
- Solvent processing
- Crosslink

Results:

- **High proton conductivity**
- **High IV performance and durability up to >1300h**
- **Future work: Improvement of stability, conductivity, IV, and durability**

Development of Water Splitting Photocatalysts for Solar Energy Conversion

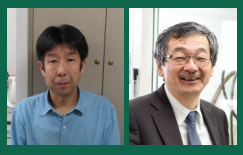

Keywords：Photocatalyst, Water splitting, Hydrogen production, Solar energy conversion

Introduction

Hydrogen produced solar driven water splitting is clean and renewable energy carrier. Direct splitting of water by photocatalysis is one of the ideal means. Nowadays, development of highly efficient and scalable water splitting photocatalysts are required.

Subjects

For efficient solar energy utilization, extension of operable wavelengths and enhancement of quantum yield are necessary. Bandgap tuning of semiconductors and control of surface redox reactions are the main strategies for materials design. In addition reactor design for bench-scale solar hydrogen production was attempted.

Design of photocatalytic materials

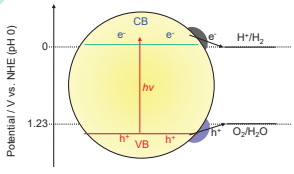

Theoretically, water splitting on a semiconductor photocatalyst proceeds with photon energy greater than 1.23 eV. However, in practice, somewhat larger photon energy is necessary due to the presence of overpotential. Most of the active photocatalysts for overall water splitting are wide-gap oxides requiring UV light excitation. To utilize much broader portion of sunlight spectrum, narrower-gap photocatalysts based on transition metal oxynitrides have been examined. Among such an attempt, $LaMg_xTa_{1-x}O_{1+3x}N_{2-3x}$ was demonstrated to be capable of overall water splitting, responding up to 600nm.

C. Pan *et. al. Angew. Chem. Int. Ed.* **2015**, *54* , 2955-2959.

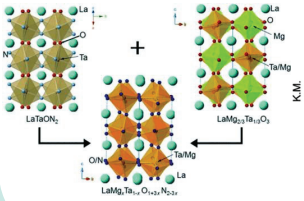

Crystal structures of $LaMg_xTa_{1-x}O_{1+3x}N_{2-3x}$

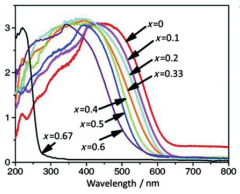

Optical properties of $LaMg_xTa_{1-x}O_{1+3x}N_{2-3x}$

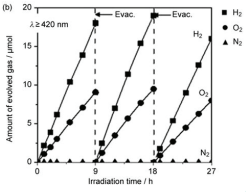

Water splitting on $LaMg_xTa_{1-x}O_{1+3x}N_{2-3x}$(x=1/3)

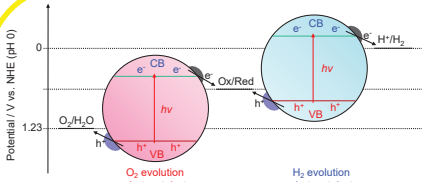

Water splitting via two-step photoexcitation combining two types of semiconductor photocatalysts mimicking photosynthesis was also examined. In this model, it is expected that relatively smaller-gap semiconductors can be utilized in terms of thermodynamics. However, this model is kinetically more challenging because the number of charge transfer steps increases compared with one-step photoexcitation route. We optimized both kinetic and thermodynamic aspects, and achieved remarkably high efficiency among the ever-reported photocatalysts by combining two types of oxide semiconductors responding up to 500nm.

Q. Wang *et. al. Nature Mater.* **2016**, *15*, 611-615

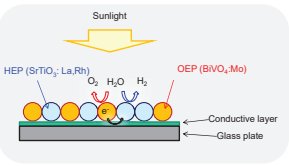

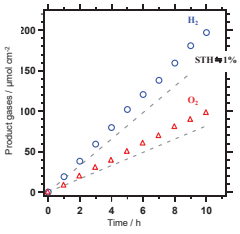

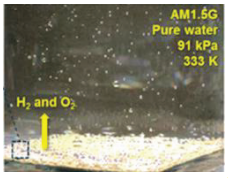

Reactor design for bench-scale test

Solar energy conversion system should be extensible to huge scale because of the low sunlight intensity. Therefore, water splitting reactor should be designed with simple structure and low cost, so that scaling up is feasible. Large size photocatalytic water splitting reactor was newly designed as a prototype of bench-scale test for sunlight driven hydrogen production.

Y. Goto *et. al. Joule*, **2018**, **2**, 1-12

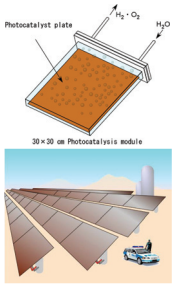

$SrTiO_3$: Representative oxide photocatalyst
BG=3.2 eV λ≦380 nm

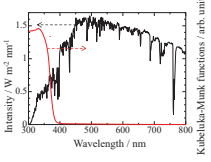

Partial overlap with sunlight spectrum
High AQY in UV region
Prototype for solar water splitting reactor

Wavelength dependence of AQY

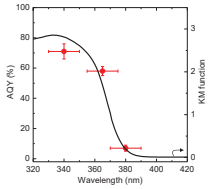

AQY=60-70%(365-340 nm)
STH=ca.0.5%
Active under real sunlight

Immobilization of photocatalyst powder

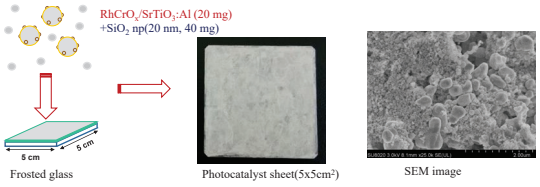

Water splitting panel (1x1 m² for field test)

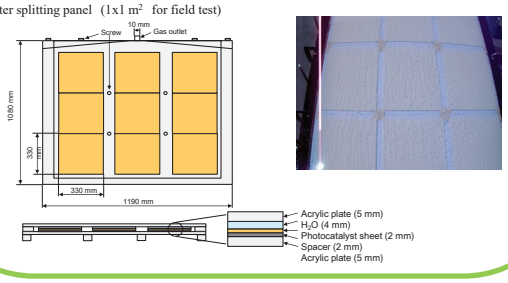

Summary

- Development of transition metal oxynitrides for water splitting responding to 600 nm. QE=ca.0.2%
- Z-scheme water splitting based on photocatalyst sheet. QE=33%, STH=1.1%
- UV-light responsive oxide. QE=ca.60%, STH=0.5%

Prospects

- Photocatalytic materials design to achieve 3～5%(STH).
- Bench-scale test for solar water splitting combining with H_2-O_2 separator.

X-Breed, Shinshu University. (GREEN, NIMS 2011～2016)

Tsuyoshi Takata, Kazunari Domen E-mail: ttakata@shinshu-u.ac.jp, domen@shinshu-u.ac.jp

P-9

Insight into the solvation structure of glyme based electrolytes via DFT-MD

Yang Sun and Ikutaro Hamada

Interface Electron Transfer Theory Group, GREEN, NIMS

Background

Glyme based solvate ionic liquid electrolytes hold the promise of achieving excellent rechargeable battery performance with high safety. Various glyme–Li electrolytes have been successfully implemented into the next generation battery technologies such as Li-S and Li-O_2 systems. The basic properties of glyme electrolytes, such as the change in solvation structure with the concentration of Li salt, have not been adequately understood.

Abstract

Density functional theory (DFT) molecular dynamics (MD) is a powerful tool to probe microscopic properties of the electrolyte. Herein we employ DFT-MD simulations to study the lithium bis(trifluoromethylsulfonyl)-amide (LiTFSI)/tetraglyme (G4) electrolyte at both low and high concentrations, and lithium bis(fluorosulfonyl)imide (LiFSA)/1,2-dimethoxyethane (DME) electrolyte at a high concentration. The solvation structure and structure-energy correlations are analyzed.

Gas phase and 1mol/L electrolyte

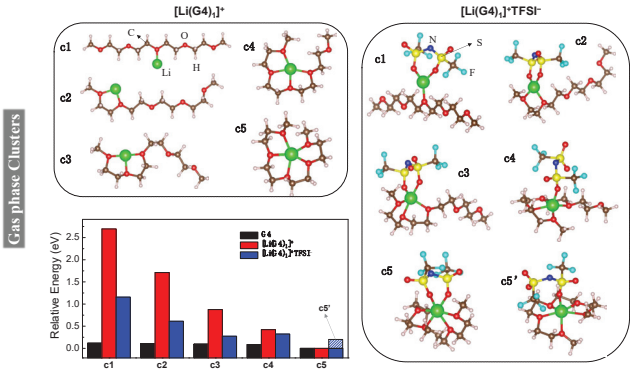

Optimized geometries of different $[Li(G4)_1]^+$ complexes and $[Li(G4)_1]^+TFSI^-$ pairs. The c*n* (*n* = 1,2,3,4,5) represents the coordination number. The total energy of G4 molecule changes very little with the conformation (curved or linear), while the stability of $[Li(G4)_1]^+$ complexes considerably increases with increasing CN and the c5-$[Li(G4)_1]^+$ complex is the most stable one.

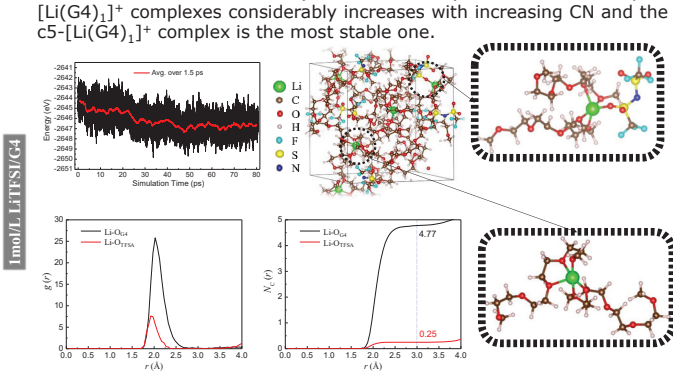

DFT-MD results of the 1mol/L LiTFSI/G4 electrolyte. The calculated CN from O_{G4} atoms is 4.76, much higher than the value from O_{TFSI} atoms (0.25), indicating that only one in four $TFSI^-$ anions is in direct contact with the solvated Li^+ ion.

Highly concentrated electrolyte

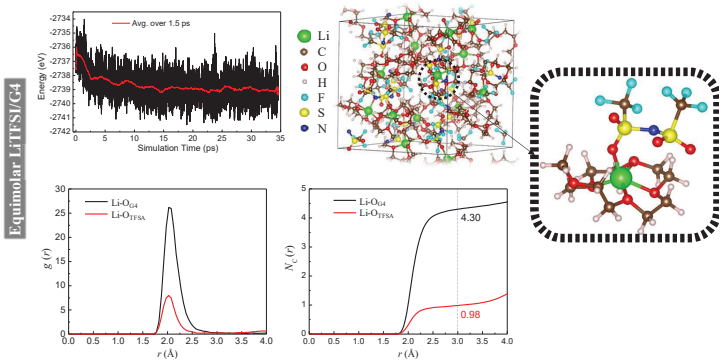

DFT-MD results of the Equimolar LiTFSI/G4 electrolyte. The Li^+ ions are predominantly coordinated by four or five oxygen atoms from one G4 molecule and one oxygen atom from one $TFSI^-$ anion, equivalent to the second most stable contact ion pair c5′-$[Li(G4)_1]^+$ $TFSI^-$ in gas phase calculations.

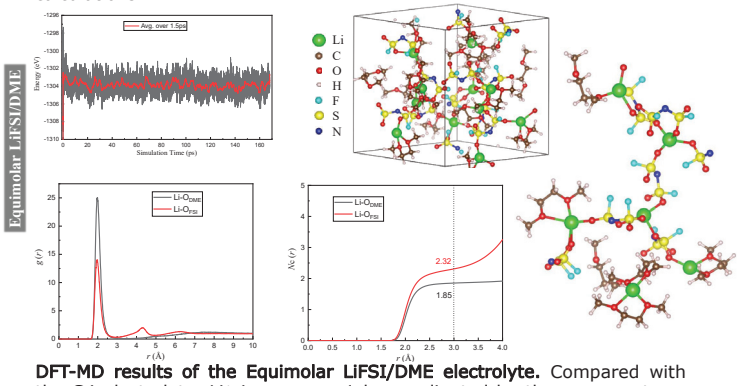

DFT-MD results of the Equimolar LiFSI/DME electrolyte. Compared with the G4 electrolyte, Li^+ ions are mainly coordinated by the oxygen atoms from FSI^- anions, mainly due to the insufficient oxygen sites of DME molecules at a high Li salt concentration.

Conclusion

- The probability of pairing between the Li-G4 complexes and $TFSI^-$ anions is significantly increased by the increased concentration of Li salt.
- At a high concentration of Li salt, the Li^+ ions are dominantly coordinated by solvent molecules in the G4 based electrolyte. In contrast, the contribution of anions to the Li^+ solvation structure prevails over that of solvent molecules in the DME based electrolyte.

Next Plan

- The dynamic (de)solvation process of Li^+ ions in tetraglyme based electrolytes.
- The transport properties of both Li^+ ion and anions.
- Interfacial reactions between tetraglyme based electrolytes and electrode materials.
- Effects of highly concentrated Li salt in different electrolyte systems.

Yang Sun and Ikutaro Hamada *J. Phys. Chem. B* 2018, 122, 10014-10022

E-mail: SUN.Yang@nims.go.jp

Electrochemical impedance analysis of the Li/Au-$Li_7La_3Zr_2O_{12}$ interface during Li dissolution/deposition cycles

Shuji Nakanishi (Osaka Univ.) and Shoichi Matsuda (NIMS)

Background

Li metal is one of the promising negative electrode materials employed in post Li-ion batteries because of its lowest redox potential and high specific capacity. However, high charge transfer resistance at the Li-electrode/LLZ interface is one of the major problems that prevents the application of LLZ in Li metal secondary batteries

Abstract

The influence of pre-coating LLZ with Au on the charge transfer resistance (***R***) at the interface of LLZ and Li is examined by AC impedance spectroscopy using a three-electrode system. ***R*** increases and decreases during Li dissolution and deposition, respectively, and the increase in ***R*** during Li dissolution is suppressed at the Li/Au-coated LLZ interface.

Experimental

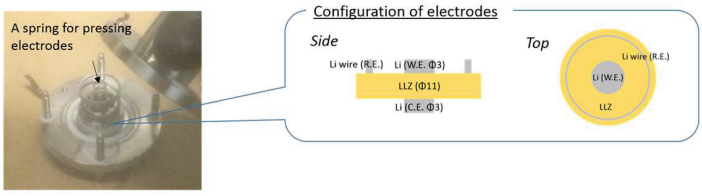

Dynamic change of *R*

R increased and decreased during Li dissolution and deposition, respectively.

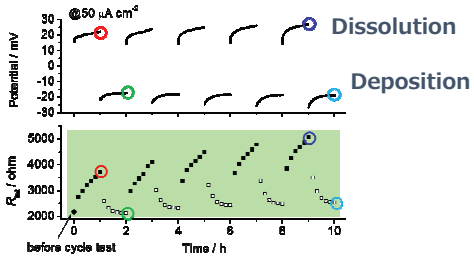

R was almost constant when Li deposition proceeded without prior Li dissolution.

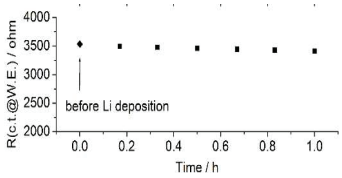

Effect of buffer layers

Au or Al layer was inserted at the Li/LLZ interface as a buffer layer.

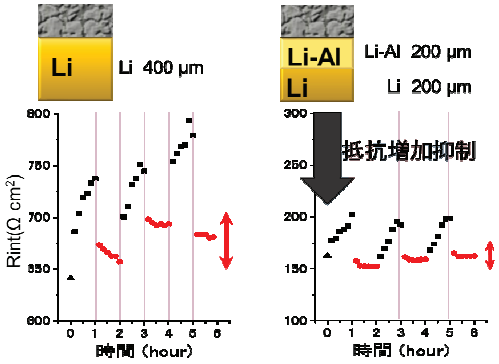

Increase of ***R*** was suppressed.

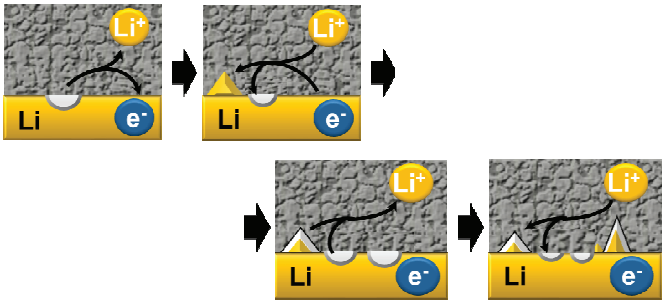

R increased (or decreased) during the dissolution (or deposition) process, suggesting that voids formed during dissolution process is the main origin of the increased ***R***.

Conclusion

AC impedance technique was employed in an attempt to trace the dynamic changes in the ***R*** at the Li/LLZ interface during Li dissolution and deposition. ***R*** increased and decreased during Li dissolution and deposition, respectively. It was suggested that the formation of voids at the Li/LLZ interface during Li dissolution is a critical factor that influences ***R***. The increase in ***R*** during Li dissolution was suppressed by the Au or Al pre-coating of the LLZ.

Journal of Electroanalytical Chemistry, 835, 143-149 (2019), ***Journal of Power Sources***, 376, 147-151 (2018).

E-mail : nakanishi@chem.es.osaka-u.ac.jp

Design of interfaces in MEA of polymer electrolyte membrane fuel cells by using quantum beam irradiation technology

Toshiyuki MORI
NIMS

Shigeharu ITO
Associate Professor
Tsutruoka KOSEN

Key Words: Fabrication, Microanalysis, Modeling, Wide three-phase boundary area

Introduction

The development of polymer electrolyte membrane (PEM) fuel cells has been the subject of particular interest for use in residential scale cogeneration systems and vehicular applications. To meet the radical innovation of fuel cell technology, the activity of Pt in the MEA should be maximized. Then, content of Pt in MEA can be in low level. For this challenge, the wide active interface area (i.e. wide three-phase boundary area) around Pt in MEA has to be designed well.

Theme under Discussion

To activate the surfaces and interfaces in the cathode layer of MEA, we try to use quantum beam (i.e. electron beam) irradiation technique. Also, we are going to design the wide three-phase boundary area around Pt in MEA on the basis of all results of microanalysis, surface atomistic simulation and fabrication route design. The present work indicates that we have great opportunity to maximize the Pt activity using metal-support interaction on CeO_x NW in MEA.

Aim of present work and suggestion from simulation

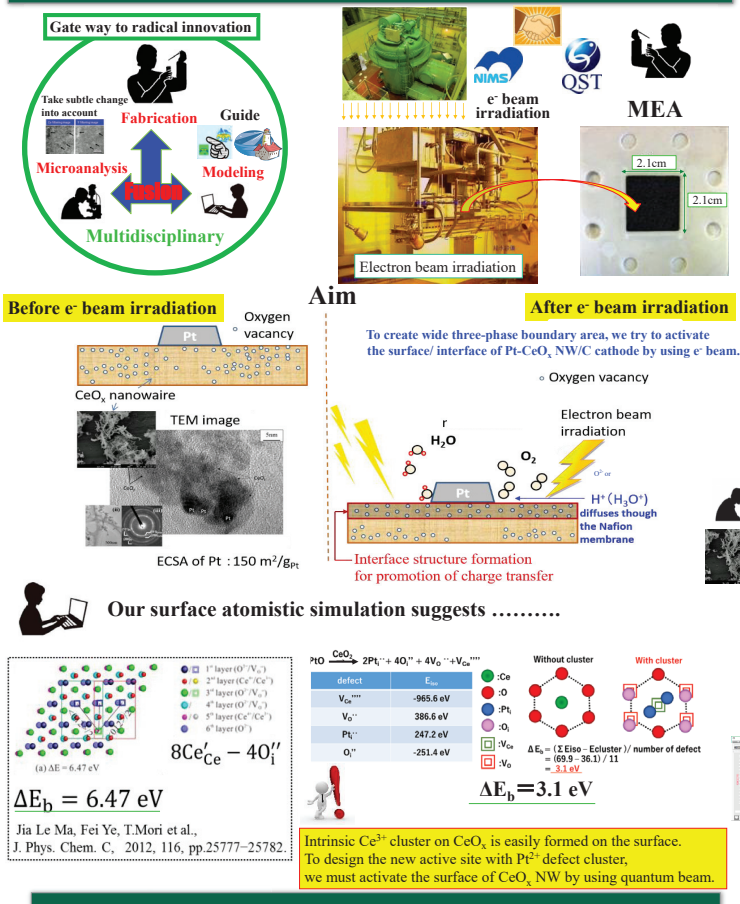

Our surface atomistic simulation suggests …….

Fabrication of wide three boundary area

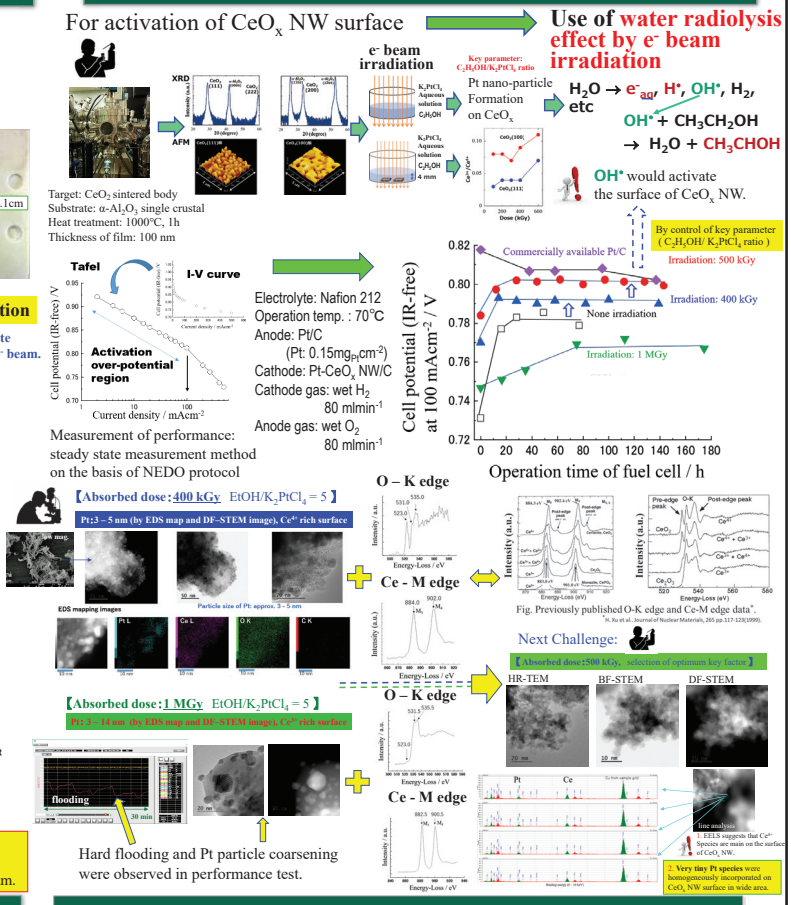

Conclusion

- The surface of CeO_x NW was activated by **e⁻ beam water radiolysis** for formation of key interfacial defect site around Pt as active three-phase boundary in cathode layer of MEA.
- The cell performance (IR-free) observed for Pt loaded CeO_x NW/C cathode in MEA was conspicuously improved by electron beam irradiation.

Future Plan

- To improve the performance of MEA, we control key fabrication parameter (i.e. C_2H_5OH/K_2PtCl_4 ratio) and evaluate the performance of MEA.
- In order to make wide three-phase boundary and maximize the performance of MEA, we will tune the interfacial defect structurer along the guide of surface atomistic simulation.

Center for Green Research on Energy and Environmental Materials,
Toshiyuki MORI E-mail: MORI.Toshiyuki@nims.go.jp on going collaboration with
Dr. Shunya YAMAMOTO (QST)

Interfacial defect structure design in IT-SOFC by multi-disciplinary approach

Toshiyuki MORI
NIMS

Shigeharu ITO
Associate Professor
Tsutruoka KOSEN

Key Words: Fabrication, Microanalysis, Modeling, High quality three-phase boundary

Introduction

Intermediate temperature (IT)- solid oxide fuel cells (SOFCs) have attracted considerable attention as a clean and efficient power source for generating electricity using air and hydrogen. If IT-SOFC provides us both of high performance and good stability around 700ºC, this challenge will give us good opportunity for development of Super-IGFC* system and guide us to the **radical innovation** for achievement of GREEN innovation .

* Super IGFC: Super Integrated coal Gasification Fuel Cells by using IT-SOFC and steam turbine engine

Theme under Discussion

To see the radical innovation in the development of IT-SOFC, the performance of IT-SOFC around 700ºC has to be improved by design of unique active sites on the anode. In the present work, we successfully designed the active sites on Ni remaining oxygen atoms or YSZ surface in anode layer (not on the cathode) by combination of fabrication route design, micro-analysis and surface atomistic simulation. We are going to develop the high quality IT-SOFC stack cells and IT-SOFC systems with industry partners in the world and 'KOSEN' national institute of technology.

New active site design on Ni in anode

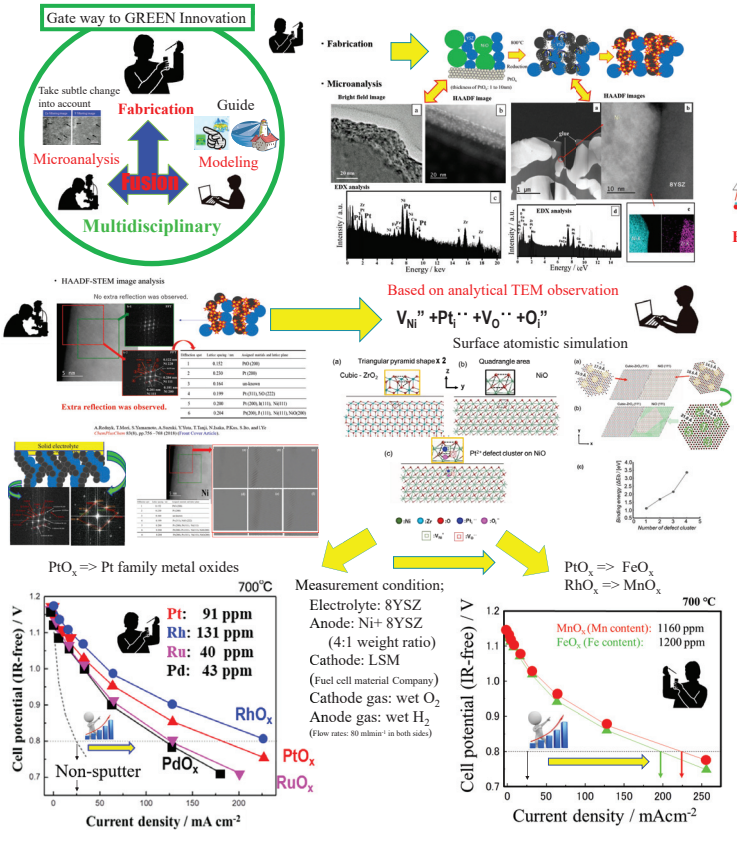

New active site design on YSZ in anode

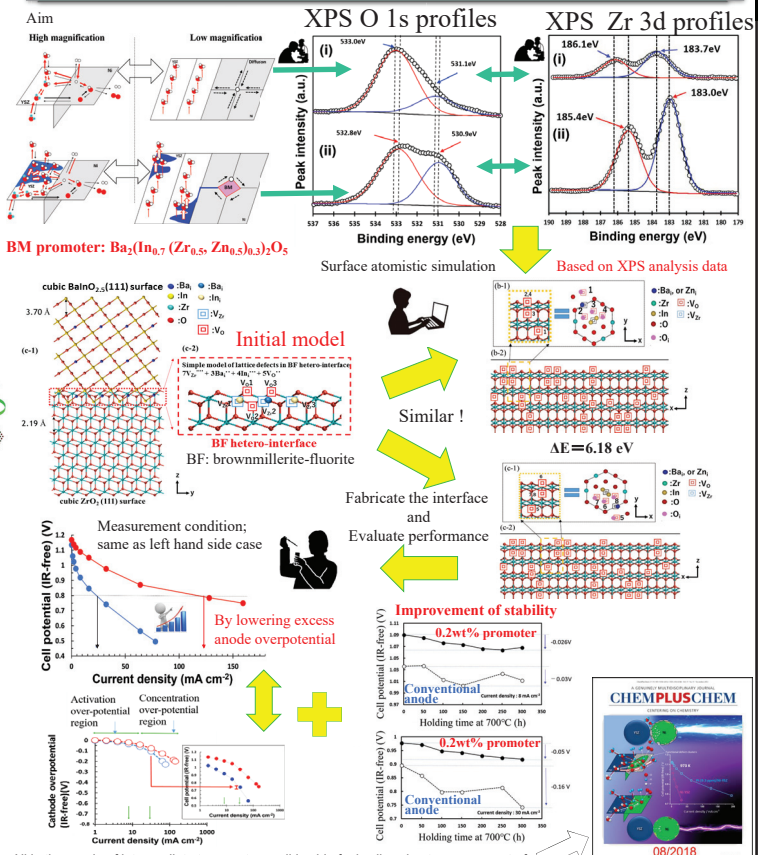

A.Rednyk, T.Mori, S.Yamamoto, A.Suzuki, Y.Yamamoto, T.Tanji, N.Isaka, P.Kus, S.Ito and F.Ye, 'Design of new active sites on Ni in the anode of intermediate temperature solid oxide fuel cells using trance amount of platinum oxides', *ChemPlusChem*, Vol.83(8), pp.756-768 (2018). (Fron cover article) Our article was selected as '2018 most accessed/ most downloaded articles in Top 20' which was announced by the Journal.

Conclusion

- Electrode performance was conspicuously improved by design of new active site on Ni and YSZ in the anode.
- New active site formation would accelerate slow surface oxygen diffusion and promote charge transfer on Ni and YSZ surfaces as predicted by recently published first principle calculation* (*S.Liu, M.Koyama et al., *J. Phys. Chem. C* 2017, 121, 19069-19079.).

Future Plan

- To maximize the performance of IT-SOFC, we are performing the **DFT + U** calculation for fine adjustment of Fe^{2+}/Fe^{3+} ratio and $Mn^{2+}/Mn^{3+}/Mn^{4+}$ ratio in the interface.
- On the basis of present results, high quality IT-SOFC stack cell and systems will be fabricated with **industry partners in the world** and **KOSEN national institute of technology**.

Solid Oxide Fuel Cell Materials Design Group, GREEN Toshiyuki MORI

E-mail: MORI.Toshiyuki@nims.go.jp

Ubiquitous-element thermoelectric materials and devices for power generation at 300~600K.



Y. Shinohara M. Goto Y. Takagiwa

Key Words: thermoelectric, ubiquitous, hybrid, high-throughput

Introduction

The targets of **Thermoelectric Materials Group** are to find ubiquitous-element thermoelectric materials with thermoelectric performance comparable to Bi-Te materials, which are suitable to power generation at 300-600 K, and to develop their power generation devices to meet social needs of exhausted heat recovery.

Theme under Discussion

- Hybrid thermoelectric materials research by Y. Shinohara.
- High-throughput investigation for energy related materials by M. Goto.
- Ubiquitous thermoelectric materials research by Y. Takagiwa.
- Thermoelectric power generation device fabrication by all members.

Hybrid thermoelectric materials

Reviewing an equation of maximum energy conversion efficiency for power generation as a basis of hybrid concept

$$\eta_{\max} = \frac{T_H - T_C}{T_H} \frac{\sqrt{1+\bar{Z}\cdot\bar{T}} - 1}{\sqrt{1+\bar{Z}\cdot\bar{T}} + T_C/T_H}$$

New hybrid concept of separation of paths for heat and current flows

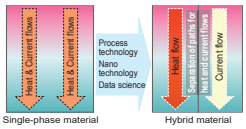

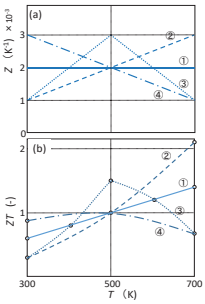

(a)Models of temperature dependence of Z, and (b)the corresponding ZT. All models indicate the same value of η_{max} between 300 and 700K, since the values of $\bar{Z}$ is same, 2X10⁻³.

Ubiquitous thermoelectric materials

Research and development of Al-Fe-Si thermoelectric material with sufficient power output based on experiment, theoretical calculation, and machine learning.

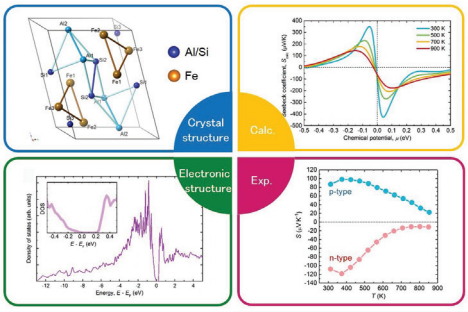

特願2017-166286,
PCT/JP2018/032031.
J. Therm. Anal. Calorim. (2018),
J. Phys. Chem. Solids (2018).

High-throughput investigation

Only one apparatus of Combinatorial Sputter Coating System (COSCOS)

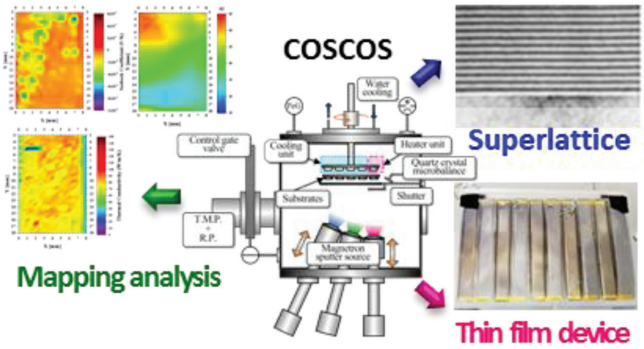

Thermoelectric devices

Fabrication of inorganic and organic thermoelectric devices for power generation by hot pressing, sputtering (COSCOS) and casting

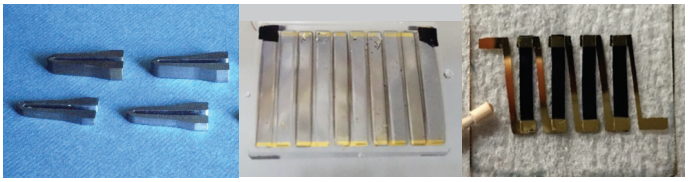

Fe-Si devices by hot pressing | Bi-Te device by COSCOS | PEDOT/PSS device by casting

Conclusion

- An reviewed equation of η_{max} was introduced.
- Operation of COSCOS has started.
- A promising ubiquitous phase was found.
- Thermoelectric devices were fabricated by different processes.

Future Plan

- The new hybrid concept is verified.
- The 3-element mapping of thermoelectric materials is promoted by COSCOS
- Thermoelectricity of the new phase is optimized.
- Electrode formation processes are developed.

Thermoelectric Materials Group, Yoshikazu Shinohara
E-mail: SHINOHARA.Yoshikazu@nims.go.jp

Molecular Design of Multi-Use Polymer Electrolyte

Key Words: Ionic liquid type polymer, Lithium-Air Battery, PEFC

Introduction

Much attention has been directed toward polymeric and ionic-liquid (IL) electrolytes and their composites for improving the safety in energy devices. We show a new concept of ionic liquid type polymers as a solid state electrolyte with a highly ion conductivity available for the Lithium-Air Battery (LAB) and the Polymer Electrolyte Fuel Cell (PEFC).

Theme under Discussion

New polymer electrolytes for the Li-Air batteries and PEFC were synthesized consisting of ionic liquid monomers. PLi(G_4)TFSMA indicated good ion conductivity, because it showed dramatic glass-transition temperature decrease than PLiTFSMA.
Additionally, we also studied efficient synthetic route for that monomer.

Anionic Polymer electrolyte

Previous reports

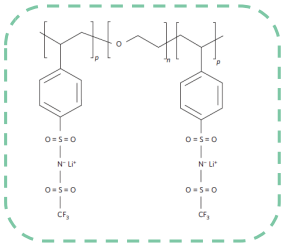

Nature Materials **2013**, *12*, 452

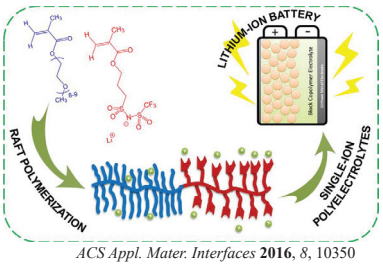

ACS Appl. Mater. Interfaces **2016**, *8*, 10350

Ionic liquid type polymer containing anionic main chain and Li^+ as free cation
Formation of block copolymer with polyethylene glycol for the purpose of promoting dissociation of Li^+ ⇒ Improved lithium ion mobility

This research

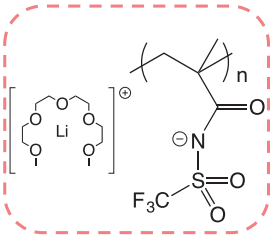

As estimated by the monomer molecular weight, improvement of Li^+ concentration is expected to be approximately 1.5 times compared with previous examples.

Polymer design concept
(1) Compact monomer ⇒ Improve Li^+ concentration in bulk
(2) Li^+ G_4 complex ⇒ Promotes dissociation of Li^+ in homopolymer

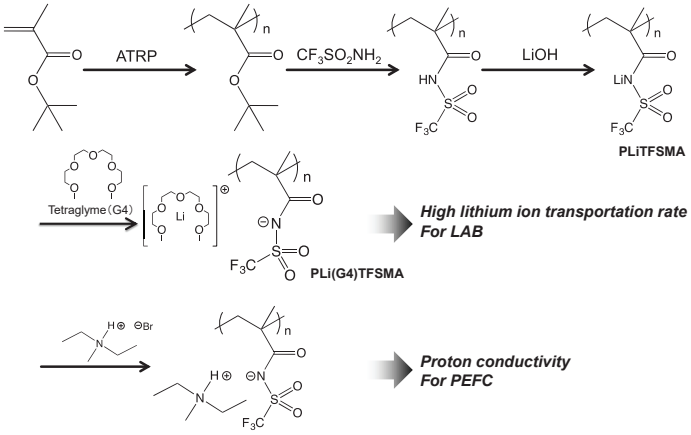

CDS soft energy

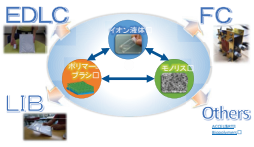

Collaborative Development Site for soft energy devices was established in April 2018 at Kosen-Applied science Research Center.
We are finding collaborators in the field of soft energy devices.

Conclusion

- We synthesized anionic main chain ionic liquid type polymer.
- For the reason the compact monomer design, polymer becomed possible to contain high Li^+ concentration.
- By using Li^+ G_4 complex, it is expected that dissociation of Li^+ is promoted in homopolymer and improve Li^+ conductivity.

Future Plan

- Li^+ containing polymer ⇒ Evaluated Li^+ conductivity and aim for implementation in lithium air battery.
- Proton containing polymer ⇒ Evaluated proton conductivity and aim for implementation in fuel cells.

Innovative Polymer Electrolyte Design Group, GREEN, NIMS
National Institute of Technology, Tsuruoka College
Ryo SHOMURA, Takashi MORINAGA, Takaya SATO* E-mail: takayasa@tsuruoka-nct.ac.jp

Vertically Aligned Tungsten Oxide Nanorods as Fast-Charging Anode for Lithium-Ion Batteries

Key Words: nanorods, lithium-ion battery, anode, cyclic voltammetry, C-rate

Introduction

Lithium-ion batteries (LIB) became an essential part of human life due to excellent combination of their properties. Today the most used anode is graphite. However, its rather low reversible capacity of 372 mAh g^{-1} results in batteries with low energy density not satisfying the demands of emerging market of electric vehicles. Therefore, there is a need to replace graphite to another active material with higher reversible capacity, lithium diffusion rate, safety, and low cost.

Theme under Discussion

Transition metal oxides (TMO) possess high capacity and cycle stability. Tungsten oxide (WO_3) with a theoretical capacity of 693 mAh g^{-1} stands out against other TMO due to combination of low cost and large volumetric capacity. WO_3 films, sheets and randomly aligned nanorods (NRs) are promising anode materials with high specific capacity and cycle performance. Here we propose to enhance the properties of WO_3 anodes by using array of vertically aligned NRs.

Experimental

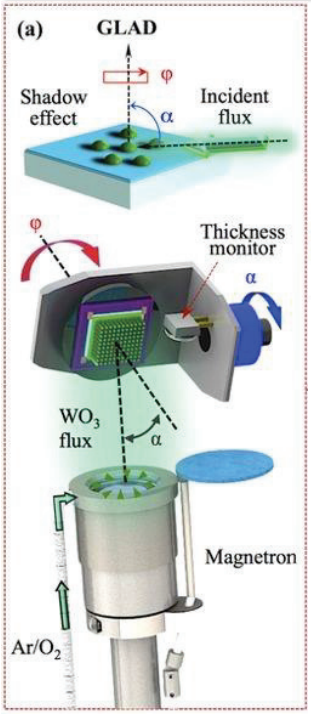

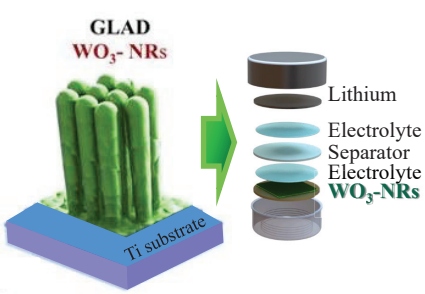

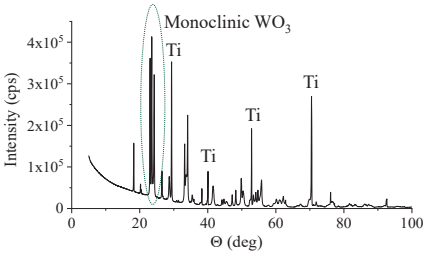

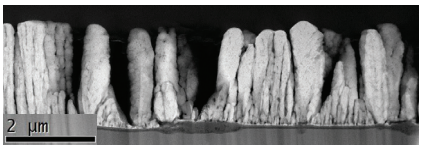

- ✓ WO_3-NRs prepared directly on the current collector by glancing angle deposition technique.
- ✓ As-prepared WO_3-NRs were tested as anode for lithium-ion batteries (LIBs).

Results & Discussion

Electrochemical Performance

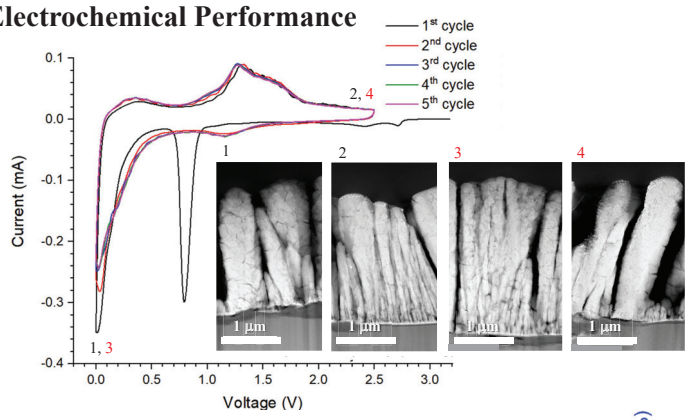

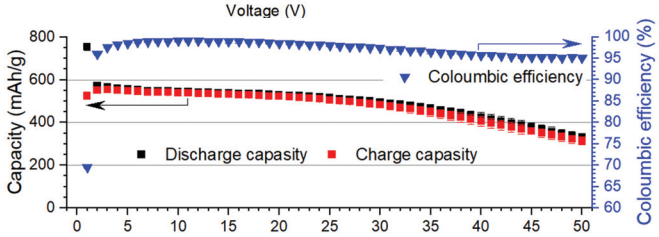

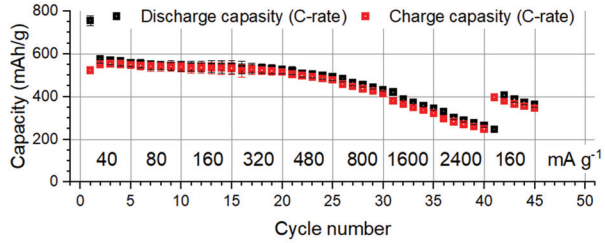

Conclusion

- Vertically aligned WO3-NRs can be used as anode for LIBs ;
- Direct synthesis on the current collector eliminated the electrical conductivity losses on the electrode – current collector interface .

Future Plan

- In-situ transmission electron microscopy study of lithiation process;
- Optimization of WO_3-NRs physical parameters: length, thickness.
- Improvement of cycle stability of WO3-NRs

In-Situ Interface Analysis Group, GREEN
Raman Bekarevich & Kazutaka Mitsuishi
E-mail: BEKAREVICH.Raman@nims.go.jp

Collaborators:
Kei Nishikawa (Metal Negative Electrodes Group, GREEN)
Yuriy Pihosh (The University of Tokyo)

In-situ Measurements on the Cathode Reaction of Lithium-Air Secondary Batteries

Key Words: Lithium-Air battery cathode, in-situ measurements, impurities

Introduction

Li-air secondary batteries (LABs) are attracting researchers' attentions because of their huge theoretical capacity. However, very low energy efficiency of cathode reactions makes LABs difficult to commercialize them. Many studies on the cathode reaction mechanism have been carried out, however, there still are many discrepancies. Further understanding on the reaction mechanism is required to develop LABs.

Theme under Discussion

Study on the reaction mechanism of LAB cathode by in-situ surface enhanced Raman scattering spectroscopy (in-situ SERS) and electrochemical quartz crystal microbalance (EQCM) measurements. The effect of electrolyte impurities on the product distribution was studied to understand the origin of the discrepancies among the studies on cathode reactions.

Experimental

Electrolyte solutions

O_2 saturated Dimethyl sulfoxide (DMSO) solutions containing 0.1 mol/L of $LiPF_6$ with different amount of impurities

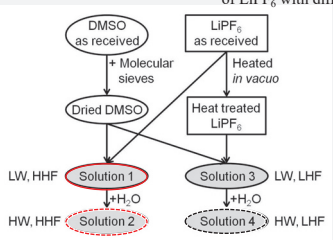

H: High content W: Water
L: Low content HF: Hydrogen fluoride

Electrolyte Solutions	$[H_2O]^a$ / ppm (mM)	$[HF]^b$ / ppm (mM)	$[F^-]^c$ / ppm (mM)
1 (LW, HHF)	5.3 (0.6)	19 (1.1)	3.0 (0.2)
2 (HW, HHF)	8.9×10^2 (59)	11 (0.7)	8.3 (0.5)
3 (LW, LHF)	9.4 (0.4)	<1 (<0.6×10^{-1})	3.7 (0.2)
4 (HW, LHF)	7.5×10^2 (50)	<1 (<0.6×10^{-1})	3.1 (0.2)

[a]Karl Fischer titration, [b] ^{1}H-NMR (Using DMSO-d_6 as a solvent), [c]Ion chromatography

In-situ SERS

WE: Au electrode modified by aggregates of Au nanoparticles
CE: Pt wire, RE: Ag/Ag$^+$
Microscope: a confocal, laser Raman, microscope (RAMANtouch, Nanophoton Corp.) with x10 objective under 785 nm excitation.

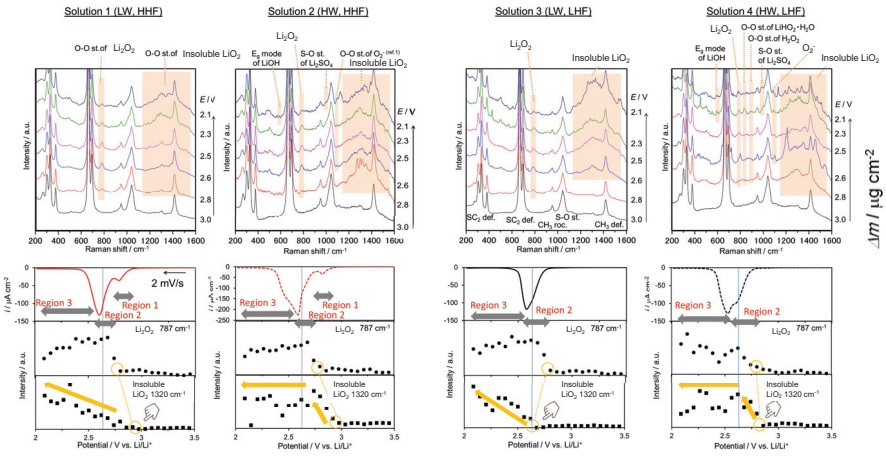

EQCM

WE: As-sputtered Au electrode on a quartz resonator
CE: Pt wire, RE: Ag/Ag$^+$
Analyzer: a QCM analyzer (QCA-922, Seiko EG&G Co., Ltd.) under 9 MHz operation.

Solution 1 (LW, HHF)
Solution 2 (HW, HHF)
Solution 3 (LW, LHF)
Solution 4 (HW, LHF)

$$\Delta F = -\frac{2 f_s^2}{N\sqrt{\mu_q \rho_q}}\Delta m - \frac{8 K_0^2 \varepsilon_{22} A f_s^2}{N^2 \pi h_q}\Delta R$$

Mass change — Viscoelastic change

ΔF: Resonance frequency shift of sharing vibration, f_S: series resonant frequency for the unperturbed QCM, μ_q: share modulus of quartz, ρ_q: density of quartz, K_0^2: the electromechanical coupling constant for quartz, ε_{22} is the quartz permittivity, A: the area of electrode, h_q: the thickness of the resonator.

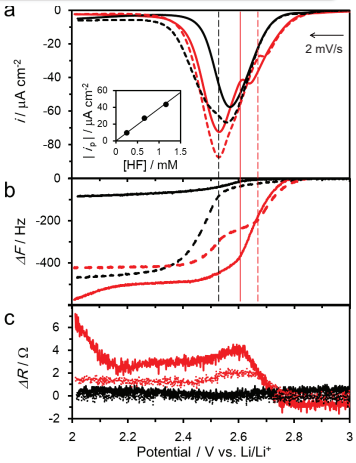

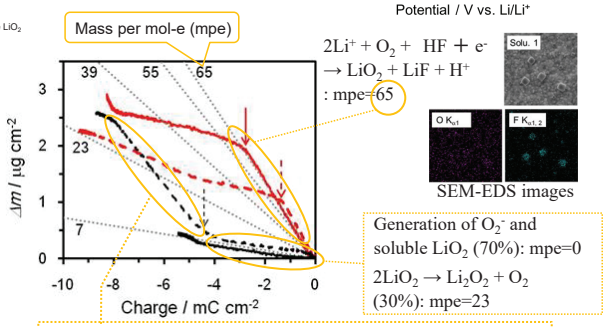

$2Li^+ + O_2 + 2e^- \rightarrow Li_2O_2$
$Li_2O_2 + H_2O \rightarrow LiHO_2 + LiOH$
$LiHO_2 + CH_3SOCH_3 \rightarrow CH_3SO_2CH_3 + LiOH$: mpe=55
$2LiOH + CH_3SO_2CH_3 + 2O_2 \rightarrow Li_2SO_4 + 2H_2O + 2HCHO$

Results

- HF caused deposition of insoluble LiO_2 at positive potential region with an equimolar amount of the LiF.
- H_2O results in the formation of $LiHO_2 \cdot H_2O$ and H_2O_2 at positive potential region, and Li_2SO_4 at negative potential region.

Conclusions

- HF in the electrolyte solution enhanced the deposition efficiency of the ORR product.
- The ORR product consisted of equimolar deposition of LiF and insoluble LiO_2.
- H_2O induced the decomposition of the solvent, DMSO.

Future Plan

- Development of the LAB system with high energy efficiency.

Maxell, Ltd., Kentaro Tomita (E-mail: kentaro.tomita.bk@maxell.co.jp)
NIMS GREEN, Hidenori Noguchi, and Kohei Uosaki

P-17

Soft X-ray Emission Spectroscopy of Crystalline and Amorphous Li_xSi Alloys in Lithium-Ion Batteries Anode

Andrey Lyalin[1], Vladimir Kuznetsov[2], Kohei Uosaki[1] and Tetsuya Taketsugu[1,3]

[1] GREEN, National Institute for Materials Science (NIMS), Tsukuba 305-0044, Japan

[2] Faculty of Physics, St . Petersburg State University, St. Petersburg 198505, Russia

[3] Department of Chemistry, Faculty of Science, Hokkaido University, Sapporo 060-0810, Japan

E-mail: LYALIN.Andrey@nims.go.jp

Introduction

Silicon is one of the promising candidates for anode materials in lithium-ion batteries (LIBs) because it exhibits more than order of magnitude greater theoretical Li capacity (4200 mAh/g for $Li_{4.4}Si$) than conventional graphite anodes (372 mAh/g). However, the high capacity of Si to host Li atoms results in a large volume expansion of about 400%, amorphization of Si, and crumbling of the electrode. To overcome this problem, one should have **detailed understanding of mechanisms of structural transformations** in Si electrodes upon lithiation/delithiation processes.

Here we demonstrate that **theoretical methods of soft X-ray emission spectroscopy** can be used as a powerful tool for the comprehensive analysis of the electronic and **structural properties of lithium silicides Li_xSi** forming in LIBs anode upon Si lithiation [1,2].

Theoretical Methods

Calculations are performed using the density functional theory (DFT) method in a plane wave (PW) basis set as implemented in the pseudopotential-based CASTEP code. We used the generalized gradient approximation with the parametrization of Perdew−Burke−Ernzerhof (PBE) for the exchange-correlation functional and the ultrasoft pseudopotentials (USPs) with two projectors for each angular momentum. The amorphous structures of Li−Si alloys were generated by the first-principles molecular dynamics (MD) simulations via the melt-and-quench scheme using the CP2K package with the mixed Gaussian and plane-waves (GPW) approach.

Intensity I(E) of an X-ray emission spectrum is given by the following expression:

$$I_0(E) = E\frac{1}{N}\sum_{n,\mathbf{k}} P_n(\mathbf{k})\delta(E - E_n(\mathbf{k}) + E_c) \quad (1)$$

where $P_n(\mathbf{k})$ is the probability of transition from n^{th} valence band to the core level c per unit time:

$$P_n(\mathbf{k}) = \frac{4}{3}\left(\frac{\omega_{nc}(\mathbf{k})}{c}\right)^3 \frac{1}{2l_c+1}\sum_{m_c,\alpha} |\langle\psi_{n\mathbf{k}}|r_\alpha|\phi_c\rangle|^2 \quad (2)$$

For further details of calculations see Ref. [1].

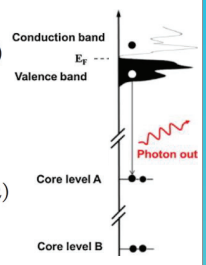

Experimental Observations

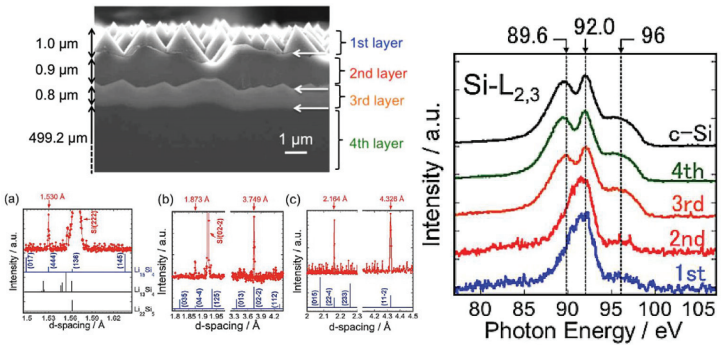

Figure 1. Cross-sectional SEM image of the lithiated Si sample, out-of-plane XRD pattern, and Si-$L_{2,3}$ XES of the 1st, 2nd, 3rd, and 4th layers of lithiated Si according to Ref. [3].

X-ray Emission Spectra of Li_xSi Alloys

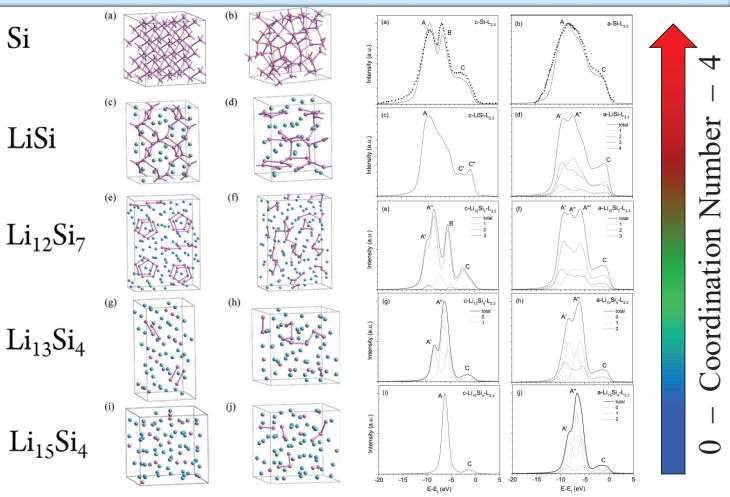

Figure 2. Optimized structures and calculated Si-$L_{2,3}$ X-ray spectra of the crystalline and amorphous phases of Si (a, b) and Li_xSi alloys: LiSi (c, d), $Li_{12}Si_7$ (e, f), $Li_{13}Si_4$ (g, h), and $Li_{15}Si_4$ (i,j). Numbers 0, 1, 2, 3, and 4 denote emission from the Si atoms with different coordination. [1]

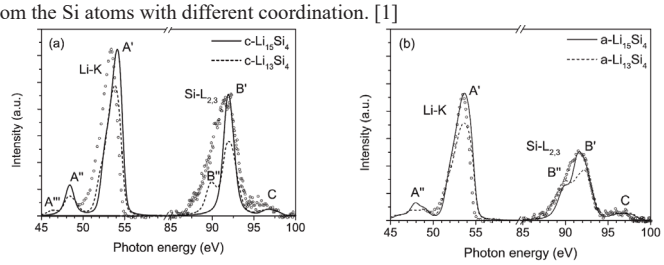

Figure 3. Soft X-ray Li-K and Si-$L_{2,3}$ emission spectra calculated for crystalline (a) and amorphous (b) phases of $Li_{15}Si_4$ and $Li_{13}Si_4$ [1,2]
Circles: experimental emission spectra of the first (a) and second (b) outermost layers of the electrochemically lithiated Si(111) [3].

Conclusions

The Si-$L_{2,3}$ emission bands of the crystalline and amorphous Li_xSi alloys show different spectral dependencies reflecting the process of disintegration of Si-Si network into Si clusters and chains of the different sizes upon Si lithiation. This feature can be used for the detailed analysis of the Si lithiation process and LIB's anode structure identification [1,2].

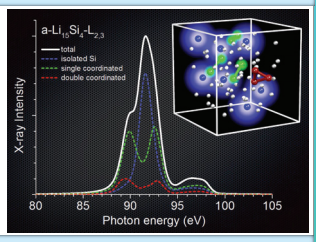

References

[1] A. Lyalin, V. Kuznetsov, A. Nakayama, I. Abarenkov, Il. Tupitsin, I. Gabis, K. Uosaki, and T. Taketsugu, *J. Phys. Chem. C* **122**, 11096 – 11108 (2018).

[2] A. Lyalin, V. Kuznetsov, A. Nakayama, I. Abarenkov, Il. Tupitsin, I. Gabis, K. Uosaki, and T. Taketsugu, *Electrochem. Soc*. **166** (3), A5362 – A5368 (2019).

[3] N. Aoki, A. Omachi, K. Uosaki, and T. Kondo, *ChemElectroChem* **3**, 959 – 965 (2016).

Advanced Low-Dimensional Nanomaterials Group



Jie Tang Hiroaki Isago Taizo Sasaki

Key Words: Graphene, CNT, Supercapacitor, Nanowire, Electron Source

Introduction

Aiming for the most sophisticated industrial use in energy storage and electron imaging, our research thrust is focused in two types of nanometerials: (i) Fundamental research on two-dimensional graphene and graphene composites for for energy storage applications in supercapacitors and (ii) Development of one-dimensional metallic compound nanowires for applications in electron

Theme under Discussion

1. Development of graphene supercapacitors with high energy density and performance improvement of graphene electrodes;
2. Theoretical search and assessment of low-dimensional materials;
3. Development of next generation field emission electron source using nanostructured rare-earth boride and carbide nanowire;
4. Fabrication and application of carbon nanotubes

Graphene Supercapacitors

① Single or two layers graphene were exfoliated from graphite by oxidation and shear method.

② Graphene were layered with CNT spacers by advanced shear process. CNT spacers inhibited restacking of graphene layers.CNTs also act as binder to improve the conductivity.

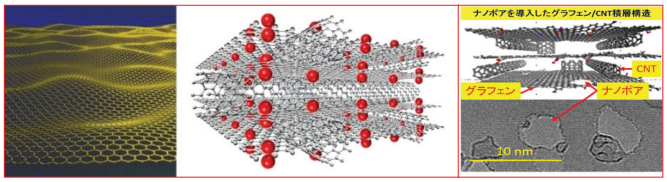

③ Energy density has nearly reached the target the power

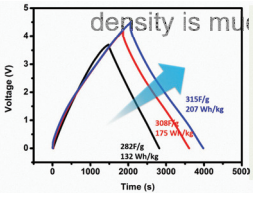

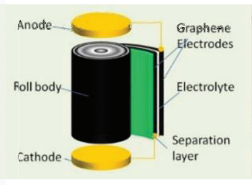

JST Advanced Low Carbon Technology Research and Development Program (JST-ALCA (H23-28))

ハリマ化成グループ HARIMA NIPPON CHEMI-CON 日本ケミコン株式会社 HONDA

MITSUBISHI PAPER MILLS LIMITED 三菱製紙株式会社 TOYO GOSEI Our Unique Approach offers Inimitable Technologies to the World.

Theoretical Search and Assessment of Low-dimensional Materials

Search of new low-dimensional materials and prediction and assessment of their properties are performed with the theoretical methods.

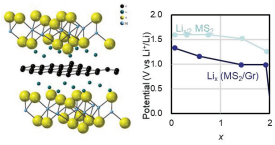

Nanostructured Electron Source

The nano-electron emitter realizing low-voltage and ultra-high brightness are also being developed.

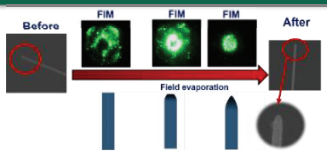

JST Development of Systems and Technology for Advanced Measurement and Analysis (H20-H25)

Collaborations:

JEOL DENKA 株式会社 日立ハイテクノロジーズ

Fabrication and Application of CNTs

Joint research with JAXA to develop CNT electron source for removing the debris in space

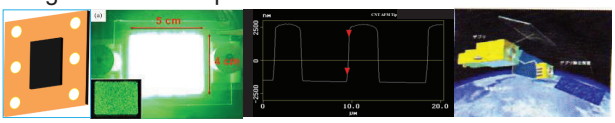

JST Matching funding program

Strengthening Capacitor Performance

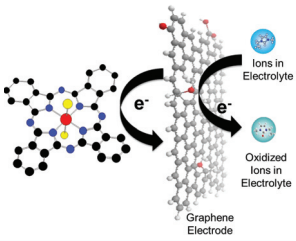

Making p-conjugate electron acceptors hybridizable with graphene electrodes to improve their performance as capacitor.

Group members

Advanced Low-Dimesional Nanomaterials Group, Jie Tang, Taizo Sasaki , Hiroaki Isago

E-mail: TANG.Jie@nims.go.jp

Center for Green Research on Energy and Environmental Materials

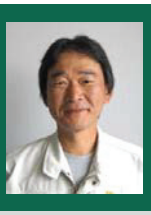

Key Words: energy creation, conversion, storage, and recovery

Objectives

Our mission is developing energy and environment-related materials for realizing energy network systems that enable us to utilize a wide variety of energy. In particular, we are developing materials for solar cells, electrochemical energy storage, hydrogen-related systems, thermo-electrics, etc.; and electrode catalysts as a common material in energy conversion among these devices with the aid of computations.

Features

This center includes Global Research Center for Environment and Energy based on Nanomaterials Science (GREEN) and NIMS Battery Research Platform; the former is a commissioned project of the Ministry of Education, Culture, Sports, Science & Technology (MEXT), and the latter is an infrastructure facility for developing next-generation batteries.

Research fields in energy value chains

Our research fields are materials science for energy creation, conversion, storage, and recovery that streamlines energy value chains.

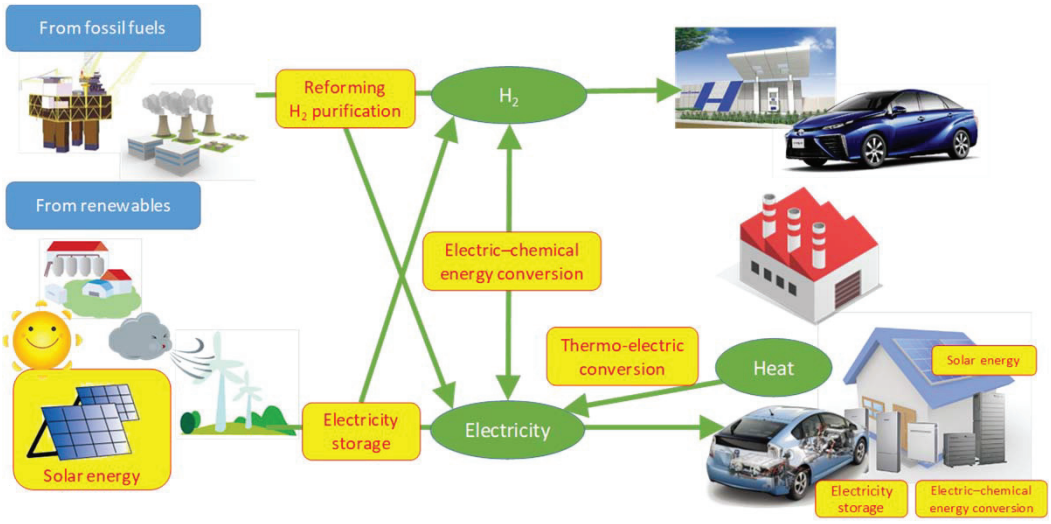

Organization

Our center consists of six research groups, four for basic research toward outputs and two for generic researches, and two innovation hubs. The materials researches in out center is accelerated by collaboration between computations, advanced measurements, and materials in GREEN; and infrastructures in NIMS Battery Research Platform.

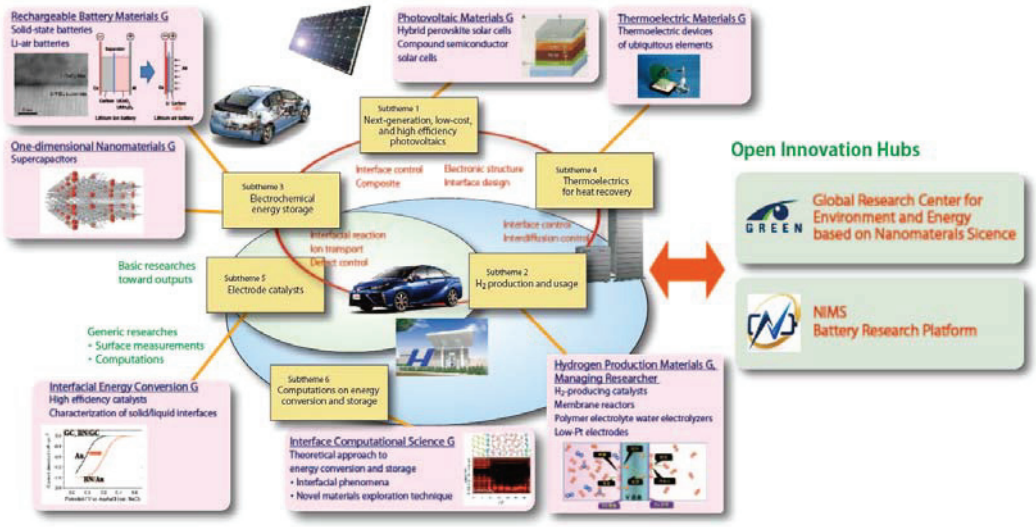

Director-General: Kazunori Takada, TAKADA.Kazunori@nims.go.jp

Deputy Director: Chikashi Nishimura, NISHIMURA.Chikashi@nims.go.jp

Rechargeable Battery Materials Group

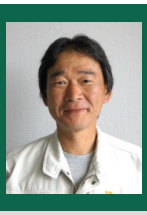

Key Words: lithium–air battery, solid-state battery, metal anode

Introduction

High energy density is required performance in rechargeable batteries. Lithium–air batteries have it theoretically; however, achieving stable cycling is a big challenge. High energy density is expected to be possible also in solid-state batteries by employing high voltage cathodes or high capacity anodes, which are not utilizable in liquid systems.

Theme under Discussion

Our research group is exploring new electrolytes with the aid of combinatorial system combined with materials informatics and developing analytical techniques to realize Li metal anodes. We are tackling grain boundary resistance in oxide electrolytes and high capacity anodes to develop high-performance solid-state batteries.

High through-put materials exploration

We have developed a high throughput combinatorial system that screens 400 samples/day automatically. We are accelerating the screening by materials informatics to achieve high performance, e.g. coulombic efficiency, in Li metal anodes.

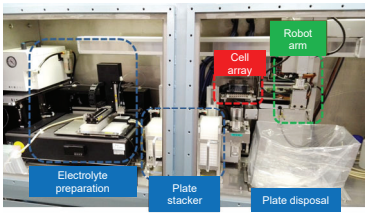

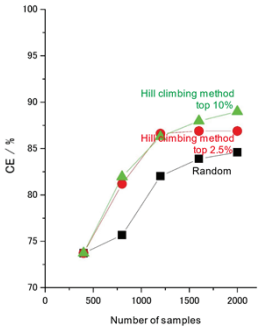

Analyzing Li anodes

Nucleation of Li metal on micro-probe electrodes

1 M $LiPF_6$/EC – DEC, i = 2 mA cm^{-2}

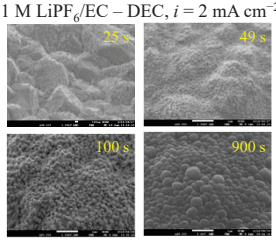

Changes in electrolyte concentration observed by interferometer

LiTFSA:G4 = 1:1

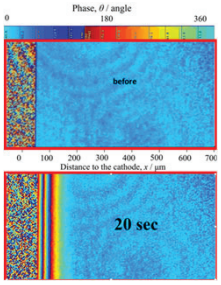

Reduction of R_{gb} in oxide electrolytes

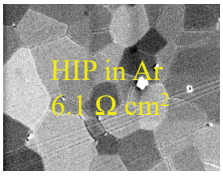

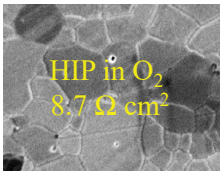

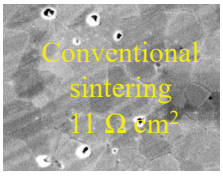

Hot isostatic pressing reduces the grain boundary resistance (R_{gb}).

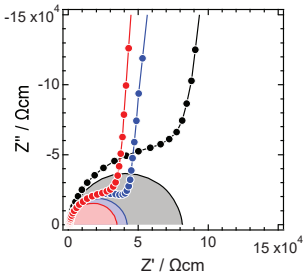

Si anode in solid-state batteries

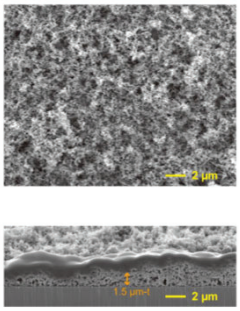

High performance of Si anodes maintains in practical form of nano particles.

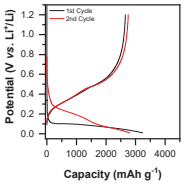

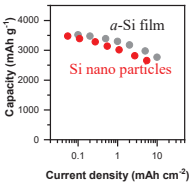

Conclusion

- The high-throughput exploration leads us to high coulombic efficiency in Li metal anodes.
- HIP reduces the grain boundary resistance to 1/2.

Future Plan

- The results from high-throughput exploration will be combined with basic research through materials informatics to develop Li/air batteries.
- Effects of the pressure on grain boundary resistance will be further investigated in order to lower the process temperature.

Rechargeable Battery Materials Group, Kazunori Takada

E-mail: takada.kazunori@nims.go.jp

Computational Study on Interfaces for the Realization of All-Solid-State Battery

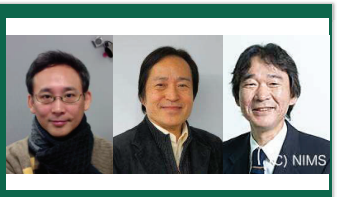

Key words: All-Solid-State Battery, Li-ion, First Principles, interface

Objective

Sulfide electrolytes are attractive attention for its high conductivity but have an issue in cyclability under the certain condition. Improved properties, however, by insertion of oxide electrolytes as buffer layers were reported. Properly combined electrodes and electrolytes are supposed to prevent unexpected charge transfer that leads no side products generation and durability of the systems. By means of first-principles, we will approach to giving the information about band alignments and interfaces which help to design appropriate applications.

Theme under Discussion

Replacing combustible liquid electrolyte with incombustible solid electrolyte is an idea of giving safety to the batteries that is all-solid-state battery systems. The issue to use all-solid-state battery systems in practice lie in the difficulties to control interfaces between inflexible solids. Using flexible sulfide electrolyte is one option to increase mechanical contact, however, those sulfide need to be treated for the better performance.

Batteries and band alignments

Oxides vs. Sulfides electrolyte

Yoshinori Tanaka, https://www.hpci-office.jp/output/hp170338/outcome.pdf

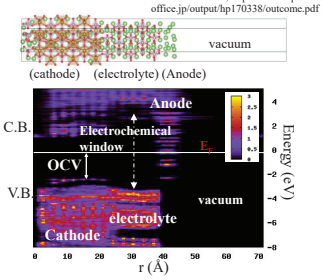

Fig.1 A mini all battery model and its calculated real space band alignment.

M. Sumita, Y. Tanaka and T. Ohno, *J. Phys. Chem. C*, **121** (2017) 9698.

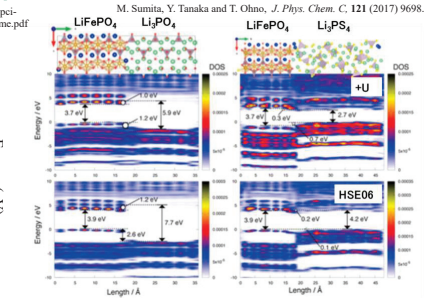

Fig.2 Calculated band alignments of half battery models. The Left is a cathode/an oxide electrolyte and the right is /a sulfide electrolyte.

The role of the interfaces in LTO

Role of interface of Anode LTO

Yoshinori Tanaka, Minoru Ikeda, Masato Sumita, Takahisa Ohno and Kazunori Takada, *J. Phys. Chem. Chem. Phys.* **18** (2016) 23383.

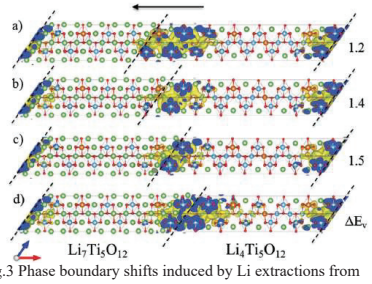

Fig.3 Phase boundary shifts induced by Li extractions from $Li_7Ti_5O_{12}$ side boundaries. Charge density around E_F is illustrated. Li atoms are extracted one by one from the (d) bottom to the (a) top. Li vacancy formation energy is listed on the side in the unit of eV.

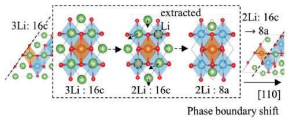

Fig.4 Schematic showing the rearrangement of Li at spinel {111} phase boundaries.

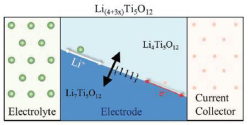

Fig.5 Schematic diagram of the role played by spinel {111}. The phase boundary provides a conduction path for electrons and Li ions. The boundaries preferentially uptake or release Li via in-plane conduction (along the white arrow) and then continuously shift in a direction perpendicular to the boundary planes (along the black arrow).

Collaborative work

Self-forming oxide buffer layer

TOYOTA

Mayuko Osaki, Hideyuki Koga and Toshiya Saito

M. Osaki, et al., Proceeding of the 2015 MRS Fall meeting, PP5.07 (2015)

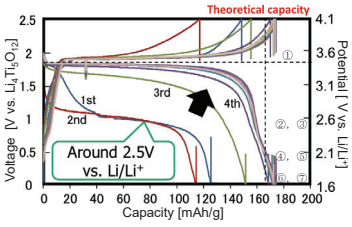

Fig.7 Charge/discharge curves of $LiFePO_4/Li_4Ti_5O_{12}$ battery

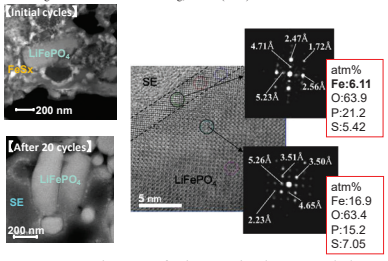

Fig.8 TEM-EDX images of $LiFePO_4$ in the SE and the electron diffraction results at the interface after 20 cycles.

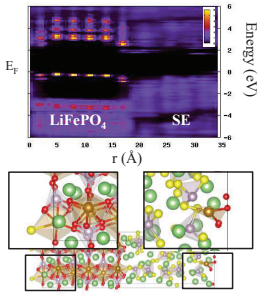

Fig.9 A stable structure of $LiFePO_4$/SE was explored by MD (below) and its band alignment was calculated (above). The results imply a sign of Fe ejection to the SE side having Fe-S bonds and absorbed Li in the cathode ($LiFePO_4$) side instead.

charge/discharge

① $FePO_4 + Li \Rightarrow LiFePO_4 + 3.4$ (eV) (3.4 V)

② $FeS_2 + 2Li \Rightarrow Li_2FeS_2 + 5.0$ (eV) (2.5 V)

③ $LiFePO_4 + Li_3PS_4 - (5/3)Li \Rightarrow (1/2)Li_4P_2O_7 + (1/6)Li_2SO_3 + FeS + (1/2)P_2S_5 + (1/3)S - 3.8$ (eV) (2.3 V)

④ $FeS + S + 2Li \Rightarrow Li_2FeS_2 + 4.1$ (eV) (2.0 V)

⑤ $FeS + P_2S_5 + 4Li \Rightarrow Fe + Li_4P_2S_6 + 7.7$ (eV) (1.9 V)

⑥ $LiFePO_4 + Li_3PS_4 - (5/3)Li \Rightarrow (1/2)Li_4P_2O_7 + (1/6)Li_2SO_3 + (2/3)FeS + (1/3)FeS_2 + (1/2)P_2S_5 - 2.7$ (eV) (1.6 V)

⑦ $Li_2FeS_2 + 2Li \Rightarrow Fe + 2Li_2S + 2.3$ (eV) (1.2 V)

For the validation of the interface reactions, the reaction formulae were evaluated by the total energy of each element and compound calculated based on density functional theory. The net energy balances associated with Li fluctuation were listed on the side.

Amorphous and crystal layers of Fe-less phosphate were self-formed at $LiFePO_4$/SE interface. The layer is considered to inhibit further side reaction at the interface.

Summary

- Band alignments were studied, for the healthy battery life.
- The roles of LTO interfaces were analysed in view of electronic and ionic conduction.
- The mechanism of the self-forming buffer layer and interface reactions were examined by the first principles MD and formation energies.

Future Prospects

- Batteries are an equipment to extract the chemical potential difference of electrons between electrodes. Firstly, overall band alignments of batteries should be concerned. Secondly, the tolerance against interface reactions should be evaluated from the view point of energetics. Properly designed batteries counting both concepts will lead to a practical application.

GREEN computation, All Solid State Battery Specially Promoted Research Team, GREEN

Y. Tanaka, T. Ohno, K. Takada E-mail : Tanaka.Yoshinori@nims.go.jp

Photovoltaic Materials Group

T. Noda A. Islam C. Niikura

Key Words: Photovoltaic, Perovskite, Quantum dot, Next-generation Si material

Introduction

Environmental issues such as global warming are an urgent one that human beings face. As a means to solve these problems, solar cells have attracted a lot of attention. To disseminate them widely in society, low cost and high efficiency solar cells are needed.

Theme under Discussion

In order to lower cost and improve efficiency, understanding of operation principle of the device and material development is important. Our group work on research aiming at elucidation of photoelectric conversion mechanism, development of new solar cell structure, and creation of new solar cell material.

Pb-frre perovskite solar cells

Sn-based perovskite solar cells, as an alternative of toxic Pb-based counterparts

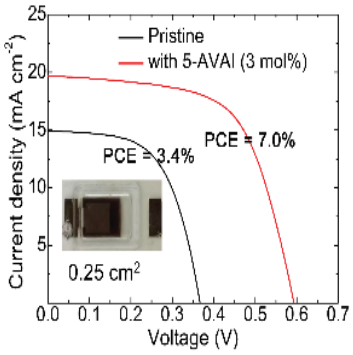

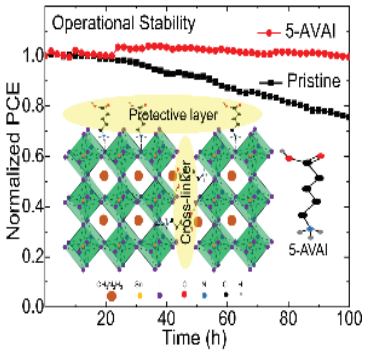

Operational stability 100h; no efficiency change

Quantum dot solar cells

high efficiency solar cells beyond the SQ limit

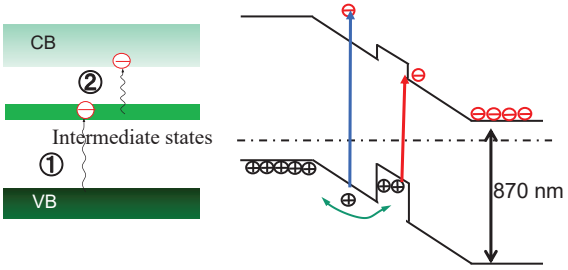

Band profiles of Intermediate band solar cell and type-II quantum dot solar cell.

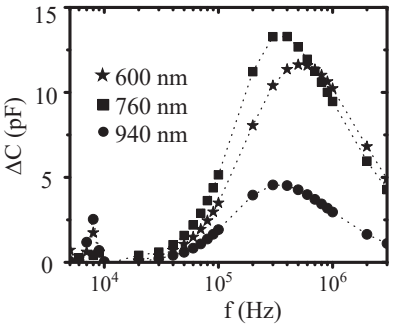

Increase of capacitance was observed, showing that accumulation of photo-generated carriers.

Next-generation Si solar cells

Aiming for low-cost and high-efficiency Si-based solar cells

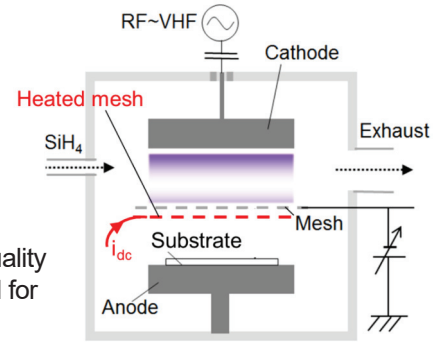

Newly developed CVD system for high-quality passivation of Si surface which is required for next-generation very-thin Si solar cells.

Conclusion

- Fabrication of Sn-based, Pb-free, perovskite solar cells
- Understanding of the dynamical properties of photo-generated carriers in QD solar cells
- An efficient Si passivation technique was proposed.

Future Plan

- Improved performance and stability of Sn-based perovskite solar cells
- Increase in the two-step photo excitation process and suppression of open circuit voltage
- Novel materials.for next-generation Si solar cells

Synthesis of $LiCoO_2$ epitaxial thin films using pulsed laser deposition

Kazunori Nishio

Rechargeable battery materials group

The tenure of period: 2010.04 – 2013.03

Introduction

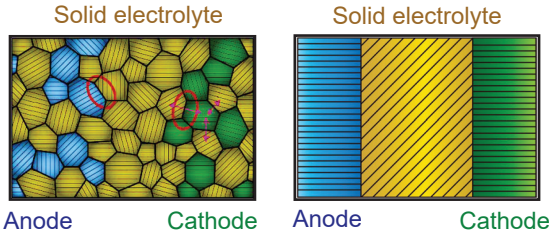

Powder-type cell Thin-film battery

All-solid-state lithium batteries have been promising energy storage devices for vehicles and smart grids due to their potential for enhanced safety and high energy density. The decrease of the interface resistance between solid electrolytes and electrode materials is of essential to achieve high power density. Despite the importance of the design and fabrication of the low resistance interface, the understandings and control of interface resistance values remain inadequate.

One approach for investigating the properties of ionic transport across the solid electrolyte and electrode interfaces is to use thin-film batteries consisting of epitaxial films. The epitaxial thin films provide well-defined interface atomic structures and crystal orientations. Accordingly, we fabricated high-quality $LiCoO_2$ epitaxial thin films using pulsed laser deposition technique.

Pulsed laser deposition (PLD)

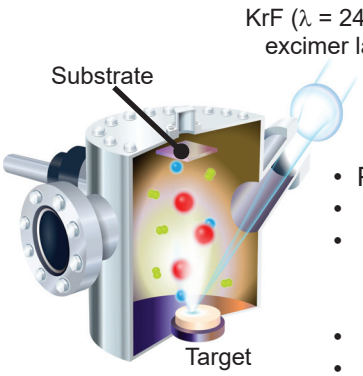

Schematically illustrated PLD

Epitaxial thin film growth parameters

- Partial oxygen pressure (P_{O2})
- Substrate temperature (T_{sub})
- Laser fluence
  1. Laser energy
  2. Spot size for target ablation
- Laser repetition rate
- Target composition

Epitaxial thin film quality is tuned by optimizing thin film growth parameters shown above.

$LiCoO_2$ crystal orientation on $SrTiO_3$

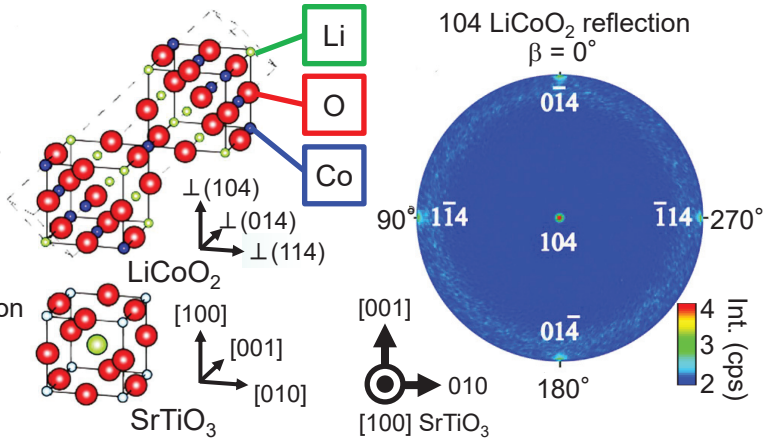

Cube-on-cube orientation relationship revealed by X-ray pole figure measurement

K. Nishio *et al.*, J. Power Sources, 247 (2014) 687-691

Crystal orientation alignment on vicinal $SrTiO_3$ (100) substrates

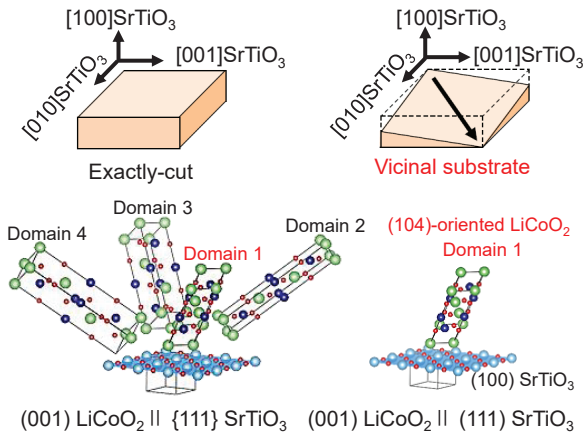

K. Nishio *et al.*, J. Power Sources, 325 (2014) 306-310.

Control of $LiCoO_2$ thin film quality

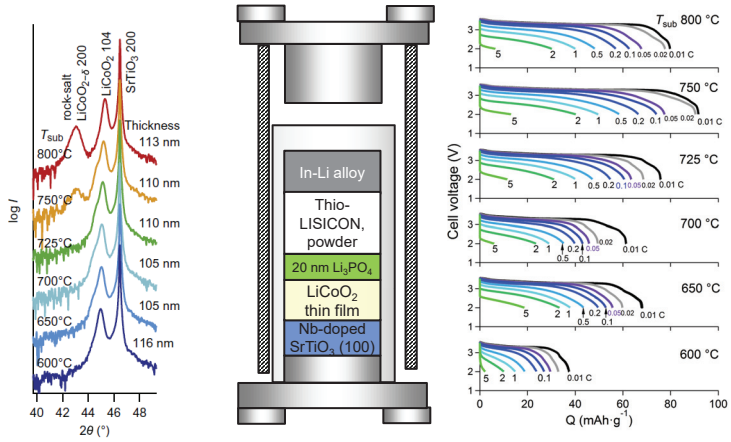

XRD patterns Fabricated solid-state Li battry Rate capability

K. Nishio *et al.*, Solid State Ionics, 285 (2016) 91-95.

Summary

- The epitaxial $LiCoO_2$ thin films were synthesized using the pulsed laser deposition technique.
- Not only the control of crystal orientations but also improving thin film quality were succeeded.
- These results highlight the importance of the preparation of high-quality $LiCoO_2$ films as a model electrode.

P-24

Optimization of the micro-grid system using the actual data of the NanoGREEN/WPI-MANA building

Technology Integration Unit, GREEN Eriko ANKYU, Karina VINK, Michihisa KOYAMA
E-mail： ANKYU.Eriko@nims.go.jp, VINK.Karina@nims.go.jp, KOYAMA.Michihisa@nims.go.jp

Introduction

A micro-grid is...

A small energy network aiming to produce, store, and consume energy locally near the consumer in order to reduce the dependency on large power generation facilities.

If the energy supply source is renewable energy (such as solar and wind power with battery)

Advantages
- Reduction of CO_2 emissions and purchased electricity
- Possibility of power supply during emergencies

Disadvantages
- Intermittent power supply because power generation depends on the weather

Previous studies

Mainly theoretical analysis
- With electricity supply/demand model
- With hourly data
- For several hours to several days

Research objective

To estimate the optimal operation of the micro-grid of the NanoGREEN/WPI-MANA building with an optimal capacity of solar power (PV) and battery, using actual data collected per second for a period of over 3 years.

Micro-grid system of NanoGREEN/WPI-MANA build.

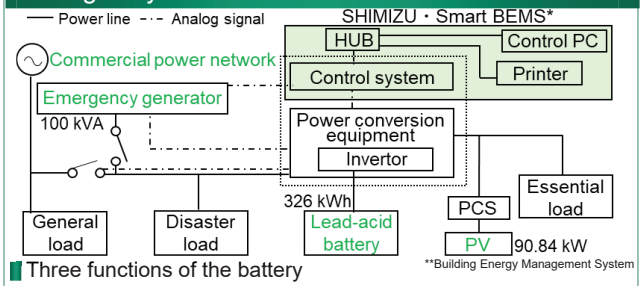

Three functions of the battery

(i) Regulating frequency fluctuation (ii) For peak cut (Jul-Sep)
(iii) As backup energy supply during emergencies

PV generation system and battery

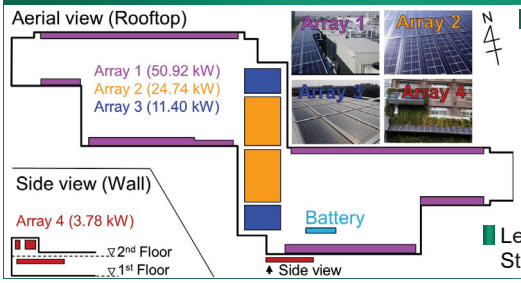

PV total capacity 90.84 kW

Array	Panel	Angle
1	monocrystal	10°
2	polycrystal	3° 357°
3	monocrystal	2° 358°
4	polycrystal	45°

Lead-acid battery 326 kWh
State of charge (SOC) 30-95%

Electricity costs

Both **contract electricity power** [kW] and **monthly energy usage amount** [kWh] should be reduced for reducing the electricity costs.

Electricity costs per month *Power factor of NIMS is 100%

= Basic rate + Energy amount rate + Renewable energy power promotion surcharge

= {Basic rate unit price×(185-Power factor*)/100+Spare wire unit price}×**Contract electricity power**
1684.8 [JPY/kW] [%] 84.24 [JPY/kW] [kW]

+ Energy amount rate unit price × **Monthly energy usage amount**
[JPY/kWh] [kWh]

+ Unit price of renewable energy power promotion surcharge × **Monthly energy usage amount**
[JPY/kWh] [kWh]

Data extraction and cleansing

Extraction of per second data (2015.1.1-2018.9.30)

1369 days×24 hours ×60 min×60 second
×12 parameter＝1,419,379,200 data

Data cleansing

1. Elimination of erroneous data
System stop with maintenance check
(On a holiday in every November)
2. Appropriate range and cleansing process
2.1.Solar power generation total
Negative value at night → 0 kW (882,281 rows)
2.2.Battery direct voltage and direct current,
Purchased electricity voltage and active power
Out of physically appropriate range → Blank
2.3.Battery SOC
Over 100% for weekly calibration → Retained
Other inappropriate data such as 0%, over 3% change per second → Blank

Parameter and appropriate range

	Unit	MAX	MIN
Battery			
Active power	kW	90	-90
Direct voltage	V	430	250
Direct current	A	360	-360
Command	kW	90	-90
SOC	%	100	30
Purchased electricity			
Voltage	V	NA	NA
Active power	kW	NA	NA
Solar power generation			
Total	kW	90.84	0
Array1	kW	50.92	0
Array2	kW	24.74	0
Array3	kW	11.40	0
Array4	kW	3.78	0

Preconditions and limiting conditions for optimization

Preconditions of battery for optimization

Battery charging from 22:00 to next day 03:00 to 100% of SOC at constant capacity, discharging from 03:00 to 22:00

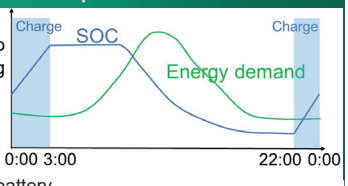

Objective function and variables

Objective function
＝MIN(annual maximum of purchased electricity)
Estimated variable is the discharge power of the battery

Limiting conditions

1) Daily total amount of the discharge of electricity per hour of battery ≦ Battery capacity
2) Discharging/charging power per hour ≦ Battery power

Assumed cases by combining different capacities of PV and battery

Original case
Actual building demand vs Actual purchased electricity

CASE1 (Optimized operation based on original conditions)
Actual building demand vs Optimized purchased electricity (1)

CASE2 (Optimized operation with PV MAX capacity*)
Actual building demand vs Optimized purchased electricity (2)

*PV MAX capacity was set as 705 kW, which was 7.8 times as large as the original PV capacity. It was calculated by the minimum value of the year of the actual energy demand divided by the PV generation.

Peak cut operation and optimization

Energy demand and purchased electricity in 2016

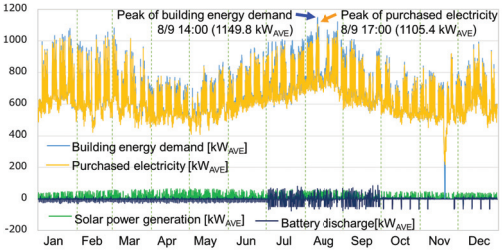

Seasonal peak day of energy demand in 2016

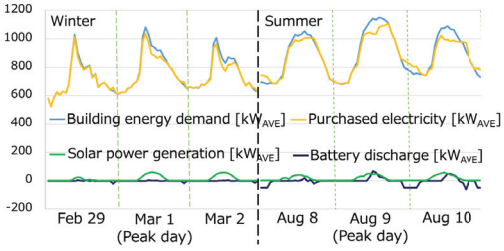

The building energy demand during weekdays in winter reached its daily peak in the morning. In the summer this is reached in the evening, and continued for a few hours.

Annual peak day during 2015-2018

	Energy demand		Purchased electricity		Diff.
Year		kW_{AVE}		kW_{AVE}	kW_{AVE}
2015	1/19 11:00	1159.1	1/21 12:00	1138.2	20.9
2016	8/9 14:00	1149.8	8/9 17:00	1105.4	44.4
2017	7/31 16:00	1141.3	7/31 16:00	1133.4	7.9
2018※	7/18 14:00	1217.0	7/18 14:00	1157.8	59.2

※By the end of Nov.

Except for 2015, the peak days of building energy demand and purchased electricity were recorded during the summer season. There was a great variation in the peak cut effect by introducing PV and battery from year to year.

Annual economic benefit in 2016

Contract electricity power：Peak cut 44.4 kW_{AVE}
Basic rate (basic rate unit price and spare wire unit price) reduction
807,531 JPY/year

＋

Monthly energy usage amount
Benefit from solar power generation
1,622,088 JPY/year
Benefit from battery operation
-102,124 JPY/year

Total 2,318,230 JPY/year

Optimal operation for reducing contract electricity power

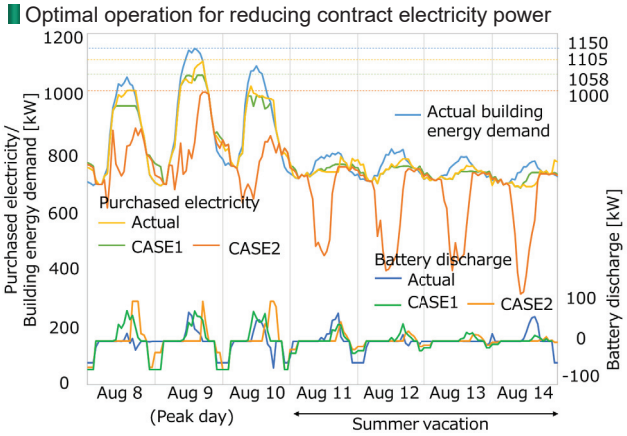

Compared to the actual building energy demand, the decrease of the purchased electricity was:
[original case] 45 kW (PV 90 kW, Battery 90 kW)
[CASE1] 92 kW (PV 90 kW, Battery 90 kW)
[CASE2] 150 kW (PV 705 kW, Battery 90 kW)

CASE1 decreased twice as much of the purchased electricity compared to the original case without investing more PV and battery. A future study could estimate the optimal point of minimizing the purchased electricity per invested amount, meaning between CASE1 and CASE2.

Conclusion

- The reduction effect of the contract electricity power of 2016 by solar power generation and battery use was approximately 800,000 JPY/year. The reduction of the monthly energy usage amount was 1,600,000 JPY/year by solar generation and -100,000 JPY/year by battery use, making a total of 2,300,000 JPY/year.
- Compared to the original case with 90 kW of PV and 90 kW of battery, the optimal operation (CASE1) would have decreased of the purchased electricity twice as much, namely by 92 kW without more investment of capacity. If the PV would have been extended to 705 kW (CASE2), the decrease of the purchased electricity would have been 150 kW.

Reference

1. Vink, K. *et al.*, Multiyear microgrid data from a research building in Tsukuba, Japan, Scientific data, DOI:10.1038/sdata.2019.20

Acknowledgement

This work was supported by the MEXT Program for Integrated Materials Development.